Master's degree project

A multi-organ single-cell transcriptomic map of the pig

Submitted by
Emilio Skarwan

Supervised by
Dr. Linn Fagerberg

5th of June, 2023
MSc Molecular Techniques in Life Science

Science for Life Laboratories
Karolinska Institutet
Stockholm University
KTH Royal Institute of Technology

Index

Abstract

Biology has a long history of drawing systematic maps of diversity. Scientific and technological advancements now made it possible to identify and describe the cellular diversity of cells based on gene expression through single-cell transcriptomics.

In this report, I discuss my work involved in the generation of a single-cell atlas of the pig based on 11 tissues and 9 brain regions. I describe my approach to data processing and cell type annotation which resulted in the generation of expression profiles for 66 cell types in the pig, based on transcript data of 186,247 cells. Additionally, I annotated all protein-coding genes in terms of their specificity to cell types. These annotations allow for the establishment of relationships between cell types and tissues based on gene expression, as well as efficient exploration of the atlas. Rigorous comparisons between pig cell types and bulk tissues as well as human cell types, indicate that the data in the atlas is consistent across datasets. However, these comparisons also highlight the need for ambient RNA data corrections procedures before a final publication.

This atlas is developed to complement the existing bulk tissue of the pig available at www.rnaatlas.org. It is expected to be a valuable reference tool for biomedical and pharmaceutical research, particularly in fields where pigs are used as established animal models. Furthermore, it has applications in agricultural research and the study and control of zoonotic diseases.

Introduction

With the widespread acceptance of cell theory in the mid-19th century and the consensus among scientists acknowledging the cell as the fundamental and indivisible unit of life, biologists have been creating maps based on the morphology and functions of cells. One notable example is Ramón y Cajal's map of cells in the nervous system.[1] In the 20th century, advancements led to the identification of DNA as the carrier of genetic information,[2] which laid the foundation for understanding how genetic information is stored and how it flows within biological systems, as proposed through Crick's sequence hypothesis and central dogma.[3] By the turn of the century, in 2001, scientists of the Human Genome Project had published most of the human genome's sequence,[4,5] which profoundly changed molecular biology research. However, this also led to the next project proposition: Sidney Brenner's *CellMap* in 2002: aiming to define cells based on the genes they express and by this create a map of all the cells in an organism, as well as the molecules within cells.[6]

Research in the last decade has followed Brenner's proposition to the letter. Advances in sequencing technologies led to the first sequencing of a single-cell transcriptome in 2009.[7] Early work by Sten Linnarsson et al. in 2011 pioneered the field by characterising 85 single cells based on their gene expression using RNA sequencing.[8] Since then, research and innovation of single-cell -omics technologies aided by computational advancements have allowed the development of large-scale multi-organ *CellMaps* or cell atlases by consortia such as the Human Protein Atlas,[9] and the Tabula Sapiens[10] each comprising thousands of cells per organ.

Although other methods exist to characterize gene expression in single cells,[11] single-cell transcriptomics has established itself as a routine method to study the gene expression activity of single cells.[12] This is due to lower costs, simpler data analysis, and high-throughput capabilities for identifying and quantifying RNA transcripts with high sensitivity.[13]

Cell characterisation through picturing a cell's RNA expression profile has led us to better understand how a diversity of cells collaborate to enable tissue and organ function.[14] It has facilitated advancements in cell development by revealing novel cell states and cell types, and at the same time it has enabled disease mechanisms to be characterised by cell malfunction.[14] Similarly, it has aided to uncover protein functions and establish reaction networks based on gene co-expression across cell types and tissues.[14] Consequently, this changed the approach of drug development by introducing novel ways to identify drug targets.[14] Single-cell transcriptomics offers a lens through which we can comprehend organ system function and dysfunction at the cellular level.

As biomedical and drug development research increasingly focuses on studying the function of the single-cell as a system, there is a growing need to describe the cells of model organisms. A baseline reference cell atlas of model organisms is essential for establishing connections between organisms at a cellular level and assessing the potential of model organisms to model a certain disease or to trial a potential treatment. Additionally, comprehensive cell atlases of livestock animals can streamline research for the prevention and control of emerging zoonotic diseases by mapping the presence of potential viral entry factors.[15]

Recognizing this need, the Human Protein Atlas (HPA) has proposed the assembly of a mammalian RNA atlas (www.rnaatlas.org), which in the future aims to incorporate both bulk and single-cell gene expression data from mammalian model organisms. The current version, however, only includes the bulk data from the pig (*Sus scrofa domesticus*) encompassing 98 tissues.[16]

The pig has become today an established model organism used in biomedical and pharmacological research.[17] Its applications span a wide range, including drug development, vaccine testing, and genome editing, as well as research in cardiovascular, dermatological, developmental, neurological, or respiratory disorders and various cancer types, among other things.[17] Despite being more challenging to handle than smaller model organisms such as rodents, pigs have higher similarities to humans in terms of size, anatomy, physiology, immunology, and tissue function.[18]

Herein, I present my work on the processing, assembling, and analysing a single-cell RNA atlas of the pig, covering 11 distinct organs and 9 brain regions based on data from Wang et al.[19], Zhu et al.[20] Zhang et al.[21] This new pig cell atlas is built using the expression profiles of 186,247 cells, which were aggregated into 66 unique consensus cell types. Throughout the project, my objectives were: (1) to investigate the cellular composition of each tissue through manual cell cluster annotation to then establish a baseline expression profile for each cell type detected; (2) to annotate all protein-coding genes in the pig based on their specificity and distribution across cell types to establish a navigable framework for the atlas and facilitating data exploration; and (3) to compare the pig single-cell-data to the bulk tissue transcriptomes and to human cell type transcriptomes to assess the quality and consistency of the data and annotations.

The pig single-cell atlas should become easily accessible at the HPA's mammalian RNA atlas (www.rnaatlas.org) and will complement the existing bulk RNA atlas.

Methods

Single-cell and single-nuclei transcriptomic datasets

The pig single-cell atlas integrates data published and generated by three previous studies[19–21] all based on tissue sections collected from three-way hybrid of Landrace, Large White, and Duroc pigs (*Sus scrofa domesticus*). In total, 24 transcript libraries stemming from 11 tissues and 9 brain regions were integrated (**Figure 1A**).

The data published by Wang et al.[19] was downloaded from the CNGB Sequence Archive of China National GeneBan Database (CNGBdb) under accession "CNP0002165". Their data provided me with both single-cell RNA sequencing (scRNA-seq) and single-nuclei RNA sequencing (snRNA-seq) datasets. For the generation of the scRNA-seq libraries, they sectioned the liver, spleen, retina, brain, lung, visceral adipose, subcutaneous adipose, and intestine tissues and isolated peripheral blood mononuclear cells (PBMC) from a six-month-old healthy pig. The brain section consisted of seven 0.5 g sections of the neocortex (cerebral cortex), cerebellar cortex (cerebellum), caudate nucleus (basal ganglia), thalamus, hypothalamus, hippocampus, hypothalamus, and pons. They constructed the library using the Single Cell 3' Gel Bead and Library kit v3 from 10x Genomics,

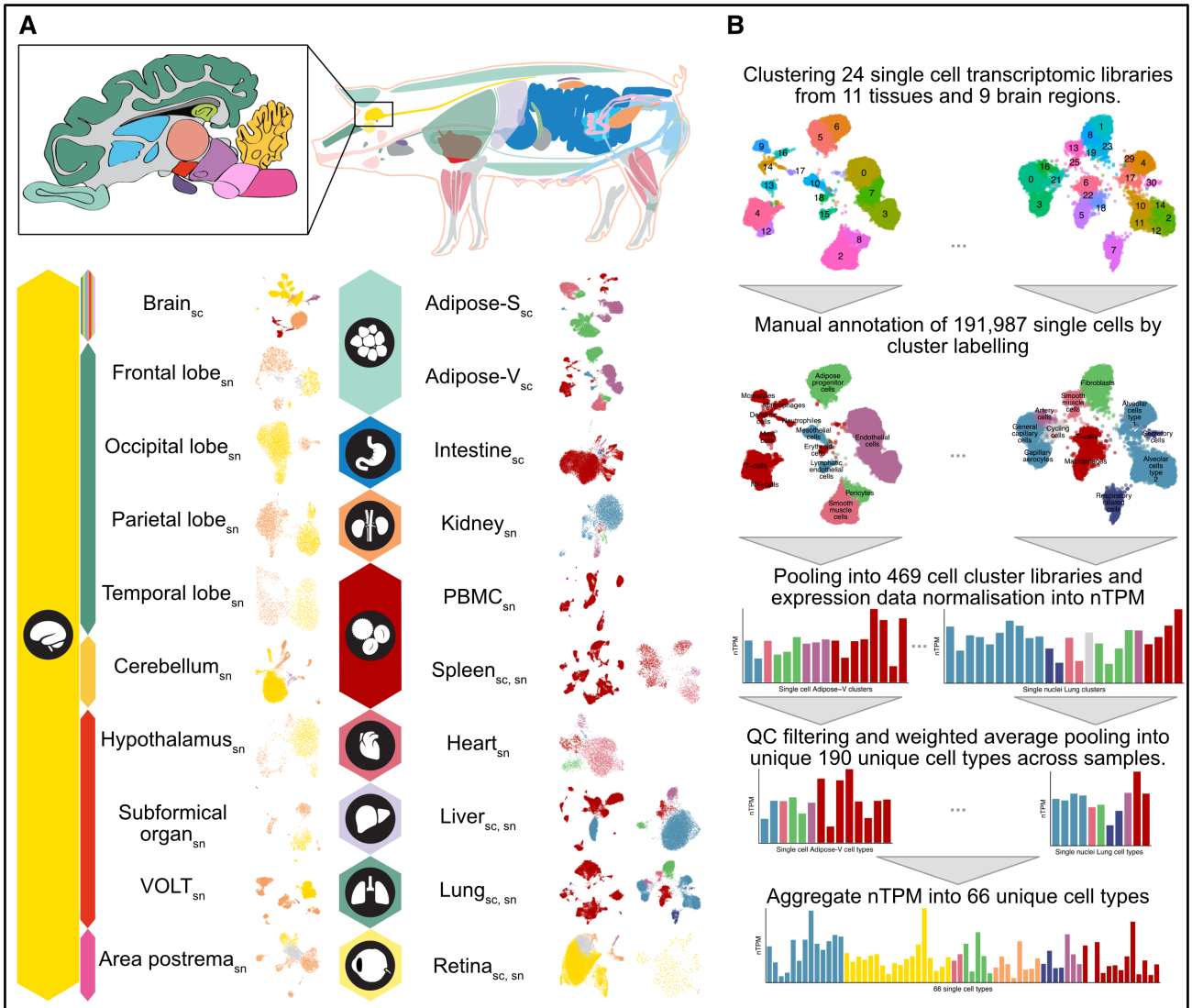

Figure 1. Overview of the single cell transcriptomic data processing. A) Overview of the datasets used for the generation of the single-cell atlas. In total 24 tissues encompassing 11 organs and 9 brain tissues were processed. Note, the brain sample, includes sections of the neocortex (cerebral cortex), cerebellar cortex (cerebellum), caudate nucleus (basal ganglia), thalamus, hypothalamus, hippocampus, hypothalamus, and pons. Illustrations of the pig and the brain, as well as the tissue symbols, were taken from Human Protein Atlas. **B)** Schematic overview of the pooling strategy applied to generate the normalised cell type expression matrix for every gene and every single-cell library.

converted the library using the MGIEasy Universal DNA preparation reaction kit (BGI), and sequenced using the DNBSEQ-T7 platform (MGI).

The snRNA-seq datasets included transcriptomic libraries from the heart, kidney, spleen, liver, retina, and four brain regions: cerebellum, subfornical organ, vascular organ of lamina terminalis (VOLT), and area postrema. These samples were sectioned from a three-month-old healthy pig. They employed the MGI DNBelab C series reagent kit (MGI) for library construction and sequenced them using the DNBSEQ-T7 platform.

The data published by Zhu et al.[20] was downloaded from CNGBdb under accession CNP0000686. They provided snRNA-seq data from five brain regions: frontal lobe, parietal lobe, temporal lobe, occipital lobe, and hypothalamus, stemming from a three-month-old healthy pig. They constructed the libraries using the Chromium Single Cell 3' Reagent Kits v2 (10x Genomics), performed library conversion using the MGIEasy Universal DNA preparation reagent kit (BGI), and sequenced them using BGISEQ-500.

The snRNA-seq dataset of the lung published by Zhang et al.[21] was accessed through CNGBdb under accession number CNP0001486. They dissected eight lung tissue pieces from three three-month-old (male) healthy pigs. Library construction was performed based on the MGI DNBelab C series reagent kit (MGI), and sequencing was done using DNBSEQ-G400 and DIPSEQ-T1 from MGI.

The sampling of all tissues mentioned above was reported as approved by their responsible ethics committees.

Preprocessing of single-cell data and cell barcode clustering

Fastq files were aligned to the *Sus scrofa* reference from Ensemble build version 109, based on the genome assembly Sscrofa 11.1 (GCA_000003025.6)[22] using cellranger 6.1.2. The filtered expression data was input into Scanpy (version 1.9.1) for downstream analysis running under Python version 3.9.5. In Scanpy, every sample underwent doublet filtering using scrublet (version 0.2.2) with an expected doublet rate set to 0.1. Outliers in terms of the percentage of mitochondrial genes detected per cell barcode were defined using median absolute deviation (MAD) thresholding, where X_i is the percentage of mitochondrial genes in a barcode:

$$MAD = median(|X_i - median(X)|)$$

Specifically, a cell barcode was considered an outlier if it exhibited more than three MADs of difference in the percentage of mitochondrial genes compared to all barcodes in the sample. Mitochondrial genes were defined as all the transcripts from the mitochondrial chromosome, as described in the Ensemble annotation.

Similarly, cell outliers were identified based on more than five MADs of difference in either the natural logarithm (log_e) of 1 + the total read counts, on log_e of 1 + the number of genes detected, or on the percentage of the top 20 most expressed genes in the sample library. Outliers were excluded from subsequent analyses. Genes detected in fewer than 20 cell barcodes containing fewer than 200 genes were filtered out.

Next, the count data was normalized to have a total of 10,000 counts per cell and underwent log1p scaling ($\log_e(1 + x)$). Highly variable genes were identified using the highly_variable_genes function in scanpy with default settings. Before cell clustering, the effect of mitochondrial genes was regressed out and PCA, neighbourhood graph construction, and UMAP were computed using default parameters based on the previously determined highly variable genes. Clusters were defined using the Leiden algorithm.

Preprocessing of single-nuclei data

For alignment, I employed STARsolo with the solotype set to CB_UMI_Simple. Additional settings were specified as follows: soloCBmatchWLtype was set to 1MM_multi_Nbase_pseudocounts, soloUMIfiltering was set to MultiGeneUMI_CR, and soloUMIdedup was set to 1MM_CR. Depending on the library preparation method (MGIEasy Universal or 10x Chromium Single cell v2), the barcode length and barcode whitelisting were adjusted to match the library.

In scanpy, singleñnuclei fastq files from the matching tissues were pooled together. The expected doublet rate in scrublet was set to 0.05 for the MGIEasy libraries. Outlier detection and filtering

followed the same rules as described above, as did the normalisation, scaling, dimensionality reduction, and clustering. Since the lung snRNA-seq sample, was the only one, which integrated sections from multiple organisms, only this sample went through batch corrections through scanpy's implementation of harmony[23] (harmony_integrate).

To note, selected snRNA-seq samples (hypothalamus, VOLT, parietal lobe, frontal lobe, area postrema, and subfornical organ) underwent re-clustering with manual settings for the calculation of variable genes, dimensionality reduction, and clustering This was necessary due to difficulties in finding a clustering pipeline that would work for all samples equally, as well as relatively low cell count in these samples.

Cell type cluster annotation

I manually annotated the resulting 469 cell clusters from the 24 libraries using scanpy. The cell transcript markers applied for cell identification were based on pig orthologs of the markers applied by the Human Protein Atlas, as well as cell markers used by Wang et al.[19] Additional markers were included through extensive literature research and used by other organ atlases. Cell type clusters that appeared to contain mixed cell types were excluded from further analysis.

Generation of cell type pseudo-bulk expression dataset and normalisation

After annotating the 469 clusters, a pseudo-bulk expression dataset was created by summing up the gene counts for each cell barcode within the same cluster. Only protein-coding genes, as defined by the Human Protein Atlas, were included in the pseudo-bulk. This resulted in a reduced expression matrix containing 22,063 protein-coding genes, for each cell cluster in a sample.

The expression count matrix of each cluster went through TPM normalisation, to obtain the protein-coding TPM expression data (pTPM):

$$RPK = \frac{gene\ count}{transcript\ length} \qquad TPM = 10^6 \frac{RPK}{\sum(RPK)}$$

The pTPM expression data was further normalized using the Trimmed mean of M values procedure (TMM).[24] To this I refer to as normalized pTPM values (nTPM). Within each sample, matching cell types were pooled together by calculating the weights, where the weights were determined by the cluster cell count. Cell clusters that exhibited mixed cell types or had low confidence annotations were excluded from the weighted average expression matrix. As a result, the number of cells effectively utilized to generate the atlas was reduced to 186,247.

Lastly, the expression profile for each cell type was computed by taking the unweighted average gene expression of matching cell types across samples. This process yielded an expression profile for 66 cell types. The processing steps following cell clustering are illustrated in **Figure 1B** for clarity.

Gene specificity and distribution classification and Tau score

The gene expression profiles of all protein-coding genes were annotated with categories that describe the specificity and distribution of the genes across cell types or tissues. The definitions for the specificity and distribution categories n be found in **Table 1** and **Table 2** below. Each protein-coding gene is assigned one specificity category and one distribution category. Genes that are cell

type enriched, group enriched, or cell type enhanced are collectively referred to as cell type elevated genes.

Specificity category	Definition
Cell type enriched	4-fold higher nTPM expression in one cell type compared to any other cell type.
Group enriched	4-fold higher mean nTPM expression of a group of 2-10 cell types (or 2-5 tissues) compared to the maximum of the remaining cell types.
Cell type enhanced	4-fold higher mean nTPM in a group (1-10 cell types or 1-5 tissues) compared to the mean expression.
Low cell type specificity	nTPM ≥ 1 and not in any of the categories above.
Not detected	nTPM < 1 in all cell types.

Table 1. Rules for assigning specificity category annotation for each gene.

Distribution category	Definition
Detected in single	nTPM ≥ 1 in a single-cell type.
Detected in some	nTPM ≥ 1 in under 31% of cell types.
Detected in many	nTPM ≥ 1 in 31% of cell types or more.
Detected in all	nTPM > 1 in all cell types.
Not detected	nTPM < 1 in all cell types.

Table 2. Rules for assigning distribution category annotation for each gene.

To complement the gene categorisation, a Tau score (τ) or tissue specificity index was calculated using a $\log_{10}(x+1)$ transformation. For every gene τ was calculated as defined by Yanai et al, where N represents the number of cell types and x_i denotes the expression value relative to the highest expression of gene i.[25]

$$\tau = \frac{\sum_{i=0}^{N}(1-x_i)}{N-1}$$

The annotations used for Figures 4, 5, 6, 7 and S6 were carried out based on 65 cell types of the pig, that is excluding platelets. The annotations used for Figure 6 were based on bulk grouped tissue data[16] from the tissues listed in Figure 6B. The annotations used for Figure S7 were based on cell type transcript data only from brain tissues and retina tissues, as well as bulk region tissue data[16] from the tissues listed in the figure. For Figure 7, the annotations of the bulk tissues were based on the whole region tissue dataset of the pig.[16] For Figure 8, the annotations were computed based on a consensus dataset aggregated as described in Figure S8, using the human single-cell data[9] and the pig single-cell data. Only pig-human orthologous genes, as defined by the Human Protein Atlas, were included in this computation.

Dimensionality reduction
The principal components (PCs) were calculated using the R package pcaMethods. The nTPM expression data was $\log_{10}(x+1)$ transformed and center scaled before performing PCA. PC1 and PC2 were used for principal component analysis (PCA) visualisation.

For UMAP visualisations, the principal components were calculated as described above ad principal components that accounted for 80% of the variability were selected. UMAP dimensionality reduction was performed using the uwot library in R, under default settings of 15 neighbours and 0.01 minimum distance.

Correlation calculations
The correlation between expression profiles was calculated using the cor function from the stats library in R, with the 'spearman' method chosen. The Spearman distance, which is 1 – Spearman correlation, was used to construct dendrograms and clustered heatmaps. Dendrograms were constructed using the hclust function from stats in R to run complete-linkage hierarchical clustering analysis on the dissimilarities. Clustered heatmaps were constructed using the pheatmap function from the pheatmap package based on the cross cell type correlation. The method complete linkage was applied for clustering.

To construct the Spearman network plot shown in Figure 7, the pairwise Spearman correlation was computed between single cells and bulk region tissues based on enriched genes using the pairwise_cor function from the widyr package. Enriched genes refer to genes annotated as cell type or tissue enriched or group enriched. Correlations under 0.60 were, and the top 3 cell type-to-tissue and tissue-to-cell type correlations were selected to build the network.

Hypergeometric tests
To compare the overlap of enhanced genes between two datasets, a hypergeometric test was performed. For this, both datasets being compared consisted of the same genes or solely of matching ortholog genes. The datasets were then categorized based on specificity and distribution. A hypergeometric test was performed by applying the function phyper from the stats package in R. In this test, q was defined as the total matching elevated genes in both datasets; m the lowest number of elevated genes between the two tissues being compared; n was the total number of genes or homolog genes subtracted by m, k was the total number of orthologs elevated in either tissue. To account for multiple comparisons, the resulting p-values were adjusted using the Benjamini-Hochberg method for false discovery rate (FDR) correction. The p.adjust function from the stats package in R was used for this correction.

Bulk pig tissue data
Pre-release data from bulk tissue transcriptomic data of the pig RNA atlas (www.rnaatlas.org), based on Ensemble build 109, were used for the comparison.[16]

Human single-cell type data
For comparisons between pig and human, the single-cell type atlas of the Human Protein Atlas[9] (www.proteinatlas.org/humanproteome/single+cell+type) was employed, based on Ensemble 103.

Batch correction using the removeBatchEffect in limma was applied before computing the UMAP shown in Figure 8C.

Data downstream analysis and visualisation

R was used for all analyses following the pTPM computation. R version 4.2.2 (2022-10-31) was run through rStudio Version 2022.12.0+353. Most visualisations were first plotted using ggplot2 (3.4.1) and edited for aesthetic and labelling purposes in affinity designer 2 (v. 2.0.4). Other packages used through R are geomtextpath (v. 0.1.1), ggraph (v. 2.1.0.9000), edgeR (v. 3.38.4), limma (v. 3.52.4), ggrepel (v. 0.9.3), patchwork (v. 1.1.2), pheatmap (v. 1.0.12), ggplotify (v. 0.1.0), plotly (v. 4.10.1), uwot (v. 0.1.14.9000), Matrix (v. 1.5-3), ggdendro (v. 0.1.23), ggalluvial (v. 0.12.5), lubridate (v. 1.9.2), forcats (v. 1.0.0), stringr (v. 1.5.0), dplyr (v. 1.1.0), purr (v. 1.0.1), readr (v. 2.1.4), tidyr (v. 1.3.0), tibble (v. 3.2.1), tidyverse (v. 2.0.0), pcaMethods (v. 1.88.0), Biobase (v. 2.56.0), BiocGenerics (v. 0.42.0), biomaRt (v. 2.52.0).

Code availability

Code applied for acquisition of data, alignment, data processing, and figure visualisation is accessible in github under github.com/emiliosk/Pig_sc_atlas.

Results

Annotating and generating baseline pig single-cell atlas data

As depicted in **Figure 1B**, I manually annotated 469 cell clusters or 191,987 cells coming from 24 libraries. The annotation processes involved referencing orthologs of cell type markers used by the Human Protein Atlas (HPA), markers used by Wang et al.[19] as well as orthologous markers used in single-cell atlases of specific organs in humans and mice. The resulting annotated UMAP plots for each transcriptomic library can be found in **Figure S1** and **Figure S2.**

Following annotation, the expression profiles of cells within each cluster were pooled together and TMM normalized to generate a pseudo-bulk expression matrix. To control for correct normalization and overall relationships between the clusters, a PCA and a UMAP plots were calculated. The UMAP and PCA plots (**Figure 2A, 2B**) demonstrate that the clusters cluster based on cell type, on tissue type, and library preparation method (snRNA-seq or scRNA-seq).

Due to differences in resolution across libraries, a standardized cell type nomenclature was established for all cell cluster names (**Figure S3**). This resulted in the detection of a total of 66 unique cell types. After quality control of the clusters, I aggregated the cluster pseudo-bulk data to form a matrix containing the expression profiles of the 66 unique cell types. This matrix constitutes the baseline expression data for the atlas and was used for all further analyses. To investigate the relationships between the transcript profiles of the detected cell types, I computed a dendrogram (**Figure 2C**). Additionally, a clustered heatmap provides detailed insights into the similarities and dissimilarities between expression profiles of all cell types (**Figure S4**).

Figure 3 summarizes the population of cell types detected in each library presented in Figures S1 and S2. Notably, there is a considerable variation in both the number of cells per cell type and the

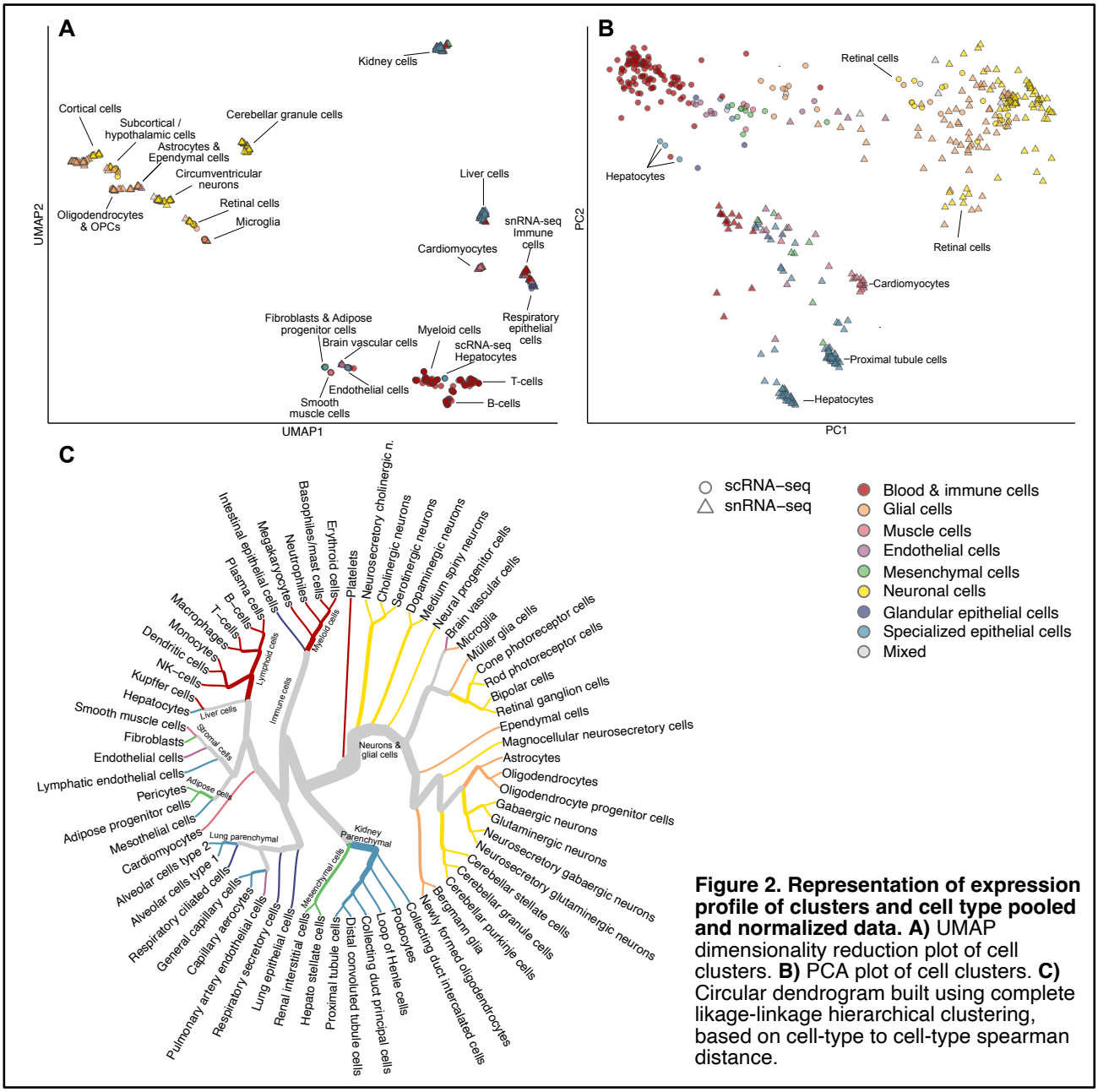

Figure 2. Representation of expression profile of clusters and cell type pooled and normalized data. A) UMAP dimensionality reduction plot of cell clusters. **B)** PCA plot of cell clusters. **C)** Circular dendrogram built using complete likage-linkage hierarchical clustering, based on cell-type to cell-type spearman distance.

number of cells in each sample. The sample with the lowest cell count (retina_snRNA-seq) amounts to only 424 cells, while the sample with the highest cell count amounts to 16,452 cells (spleen_scRNA-seq). Generally, scRNA-seq libraries yielded a higher number of cells. The cell type with the highest cell count on the other hand were T cells (N = 27,811) followed by B-cells (N = 13,481) and hepatocytes (N = 12,133). Megakaryocytes had the lowest population count (N = 16). **Figure S5** presents the relative cell count for each tissue.

Finally, to demonstrate the practical applications of the atlas based on pseudo-bulked cell type data, I programmed an atlas enquiry interface. **Figure 9** showcases examples of three out of the 22,063 protein-coding genes that can be queried through this atlas.

Annotation of protein-coding genes

Having the aggregated expression matrix in place for every cell type, I proceeded with the whole genome annotation of protein-coding genes of the pig. Each protein-coding gene was assigned a category based on cell type distribution and cell type specificity (**Figure 4**).

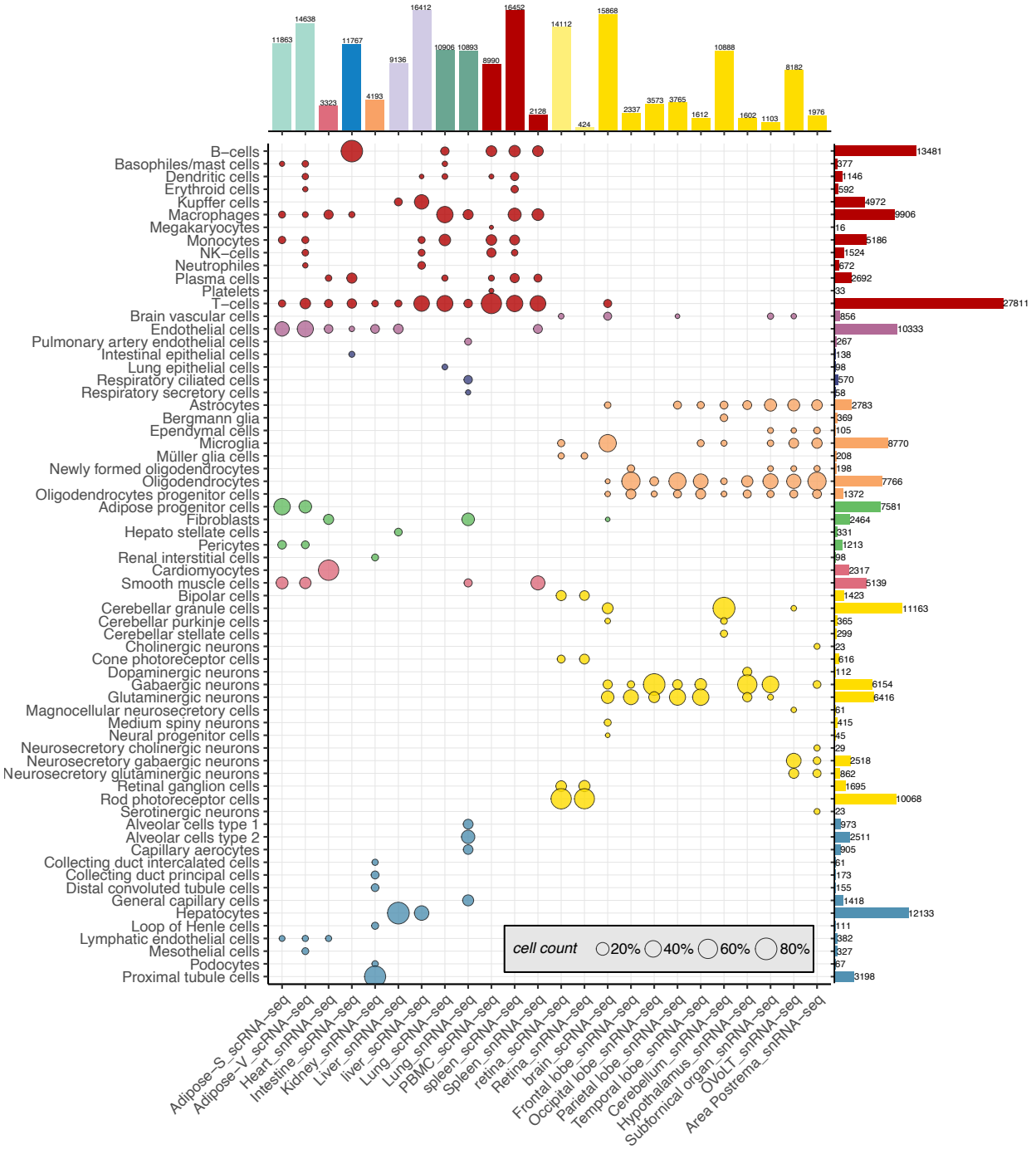

Figure 3. Cell counts identified for each cell type by sample. A total of 66 cell types were identified across all 24 libraries. Relative cell count was calculated as the quotient of the counts per cell type in a sample and the total cell count of a sample. The barplots depict the total cell count in each sample (top) and each cell type (right).

Briefly, the distribution categories are detected in single, detected in some, detected in many, detected in all, and not detected. These categorizations reveal that from the 22,063 protein-coding genes of the pig, 1,643 (7.4%) genes were not detected. Similarly, 2,440 (11.1%) genes got detected in all cells. And 1,070 (4.8%) genes were detected in a single cell type (**Figure 4A**). The cell type detected with the lowest number of genes were platelets (N = 2,756), but they were not included in the annotations due to their low gene count. Otherwise, neurosecretory cholinergic neurons were the cell type with the fewest genes, with 6,929 genes. The cell type with the highest number of detected genes were alveolar type 2 cells with 15,290. The average number of genes detected in a cell type is 12,293.15 genes (**Figure S6A**). Alveolar type 2 cells had the highest number

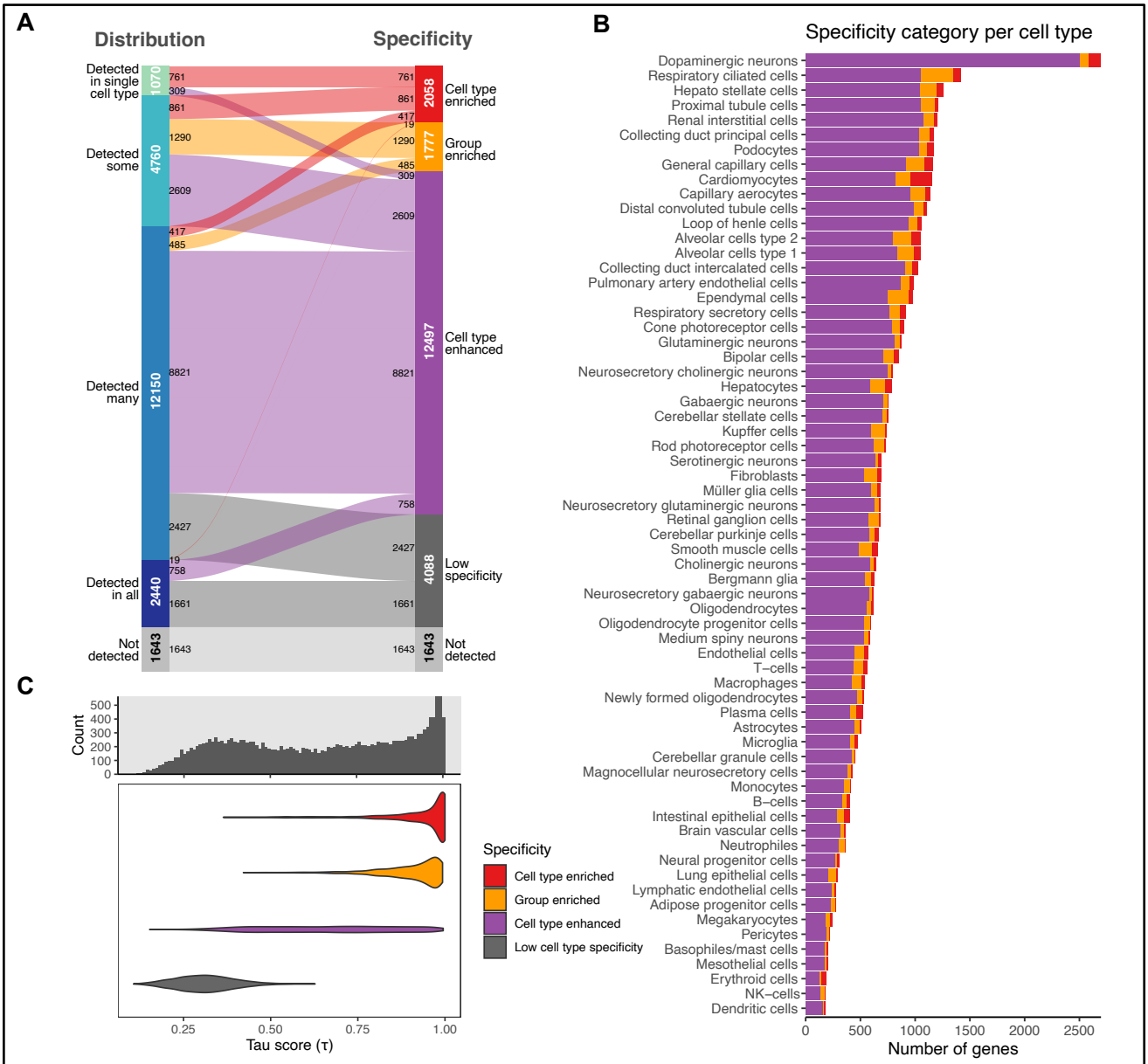

Figure 4. Distribution, Specificity and Tau (τ) specificity index annotation of protein coding genes. A) Alluvial plot depicting the number of assigned genes for each of the five distribution categories and five specificity categories, as well as the number of the number of genes in every specificity and distribution category combination. **B)** Bar plot showing the number cell type elevated genes (cell type enriched, group enriched and cell type enhanced) per cell type. **C)** Bottom, a violin plot depicting the tau scores for each gene inside split by specificity category. Top, a histogram depicting the total distribution of tau scores in the single cell dataset.

of genes detected in single a cell type (N = 107), followed by the general capillary cells (N = 90) and cardiomyocytes (N = 70) (**Figure S6B**).

Regarding cell type specificity, genes were assigned to categories ranging from highest to lowest specificity: cell type enriched, group enriched, cell type enhanced, and low cell type specificity. Only 18.5% of genes (4,088 genes) show low cell type specificity. Most genes (12,497 or 56.6%) however show to be categorized as tissue enhanced. Additionally, 8.1% (1,777 genes) are group enriched and 9.3% (2,058 genes) are cell type enriched. The number of elevated genes per cell type ranges from 184 for dendritic cells and NK-cells, up to 1,417 for respiratory ciliated cells and 2,697 for dopaminergic neurons. (**Figure 4B**). Specifically, the tissue with the lowest tissue cell type enriched genes (in red) are neutrophiles and pericytes with only two cell type enriched genes each. While the top three cell types with the highest tissue enriched genes are dopaminergic neurons with

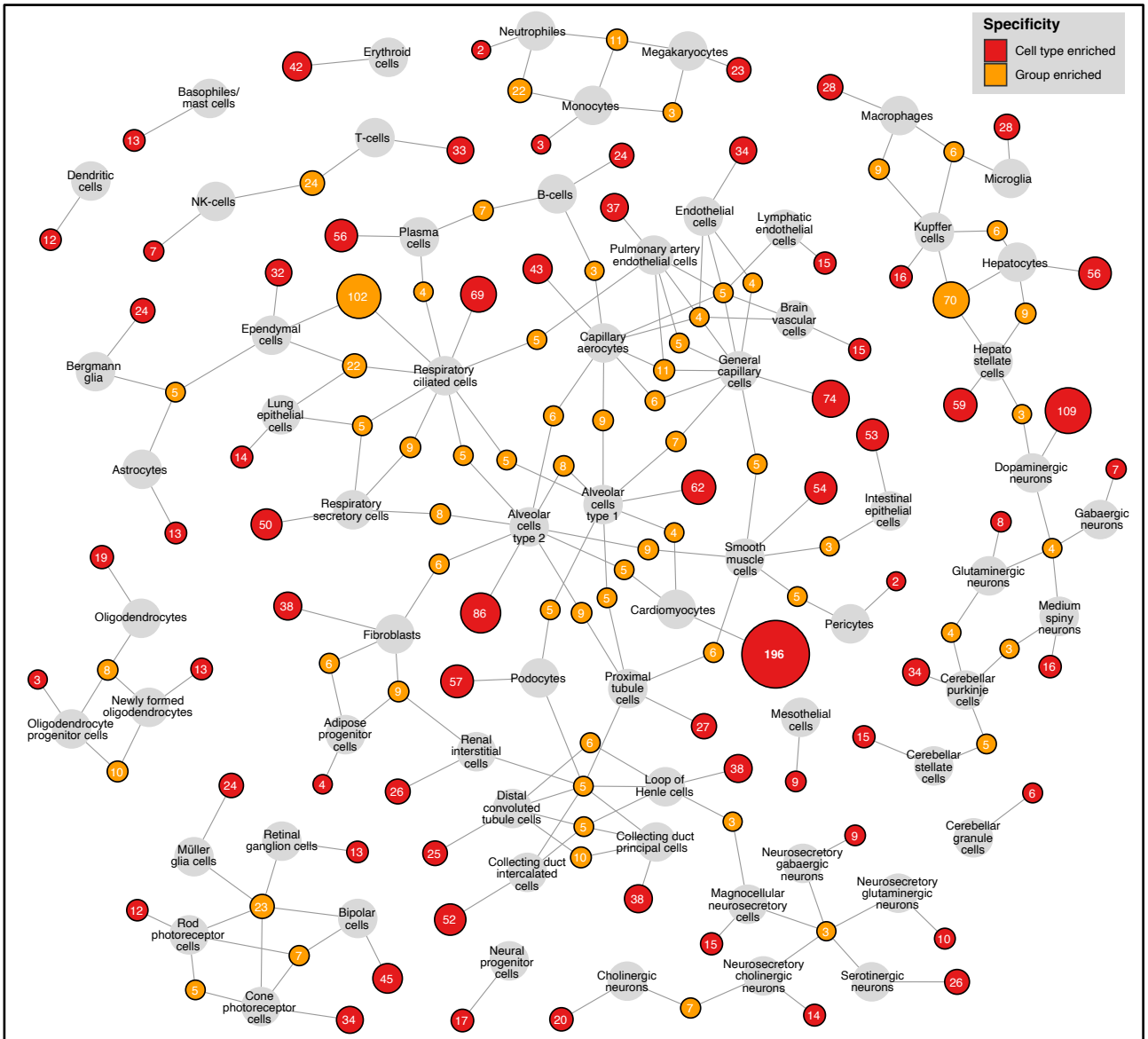

Figure 5. Network plot build upon shared group enriched genes between cell types. Additionally, for each cell type a node labelled with the number of cell type enriched genes is assigned. To reduce visual complexity, depicted are only group enriched node containing at least 5 genes or group enriched nodes which ranked top 2 for a given cell type provided they accounted with 3 or more group enriched genes.

109 and cardiomyocytes with 196. It is worth noting that, these dopaminergic neurons, are hypothalamic dopaminergic neurons, no other exclusively dopaminergic neurons were detected.

As a complement to the discrete category annotations, the numerical specificity index Tau (τ) was also assigned to every gene. As we see in **Figure 4C** a higher specificity category is usually accompanied by a high Tau score, the opposite is true as well.

As mentioned previously, gene annotation was introduced to facilitate navigation and exploration of the atlas. The annotations allow for highlighting relationships between cells through shared enriched genes. Thus, I aimed to investigate the relationships resulting from the specificity categorizations and shared enriched genes between cell types. A network plot (**Figure 5**) shows for every cell type the number of assigned cell type enriched genes in red, and the shared group enriched genes shared between cell types in orange. This plot highlights, that ependymal cells in the brain and respiratory ciliated cells in the lung share the highest amount of group enriched genes (N = 102). Similarly, the cells in the liver hepato stellate cells, hepatocytes, and Kupffer cells share

70 group enriched genes. These shared enriched genes between cell types can subsequently be explored in detail inside the atlas as exemplified in **Figure 9C.**

Comparison to pig bulk tissue data

To assess the quality and consistency of the data, I conducted a comparison between transcriptomic profiles of the cell types and the profiles of bulk tissues of the pig. For the first part of the comparison, I aimed to determine how well the single-cell data complemented the existing bulk tissue data. I compared the single-cell type data with the transcript data of the matching tissues of origin. In other words, I compare the single cell type data with the transcriptomes of the brain, retina, kidney liver, adipose tissue, heart, large intestine, small intestine, lung, and lymphoid tissue. However, the transcriptomic bulk data of the PBMC were unavailable.

As the core for my comparison, I annotated all genes in terms of specificity for the bulk tissue dataset based solely on the expression profile of the tissues mentioned above (**Figure 6A**). There are two things immediately visible after comparing the annotations of genes based on single-cell

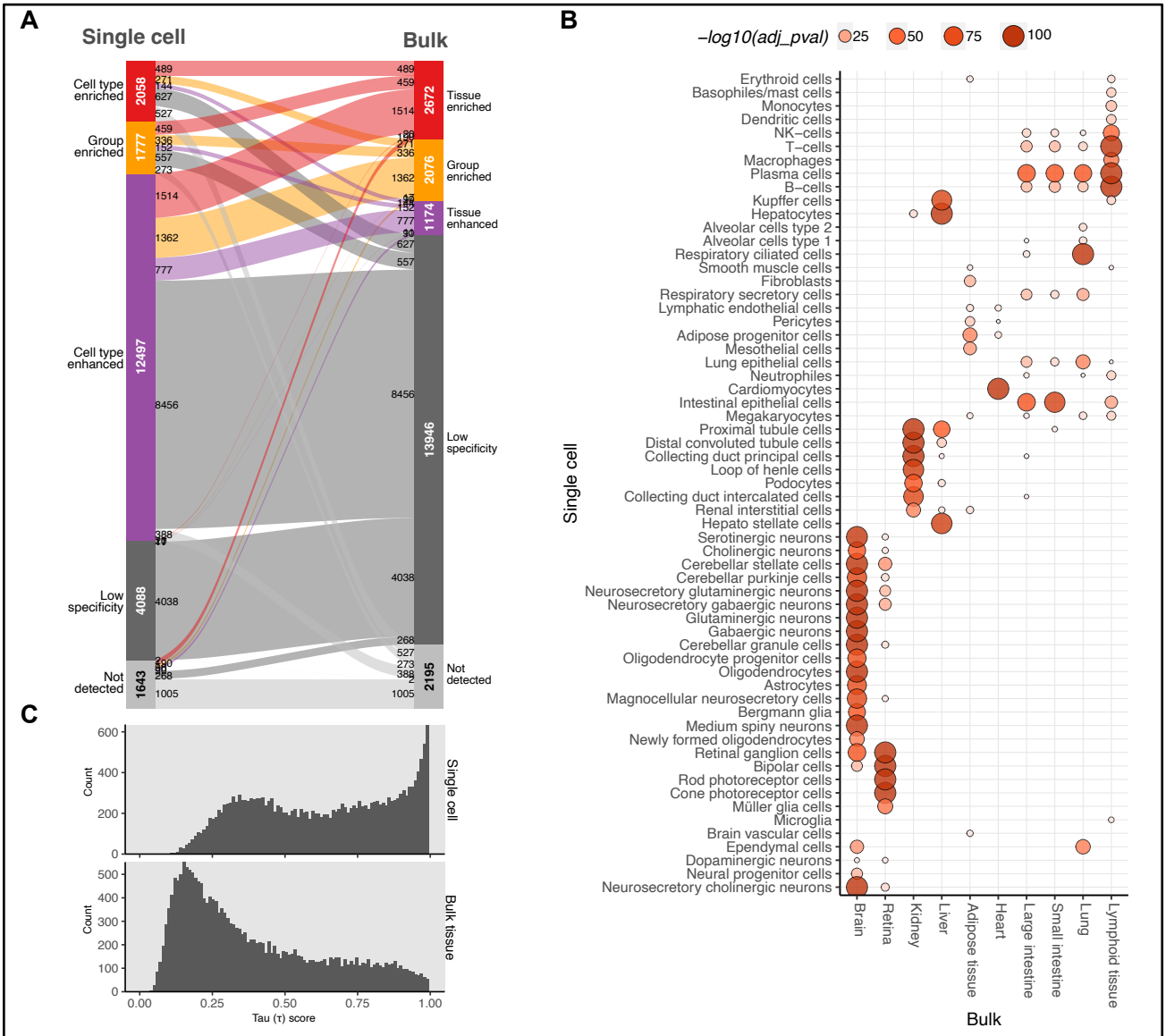

Figure 6. Comparison between bulk transcriptomic data and single cell pig data. A) Alluvial plot comparing the assigned specificity categories based on bulk data and single cell data. Note that the classification for the bulk data was calculated solely on data composed of brain, retina, kidney, liver, adipose tissue, large intestine, lung and lymphoid tissue data. **B)** Hypergeometric test, based on matching elevated genes between tissues and cell types. **C)** Comparison between Tau scores computed using both datasets.

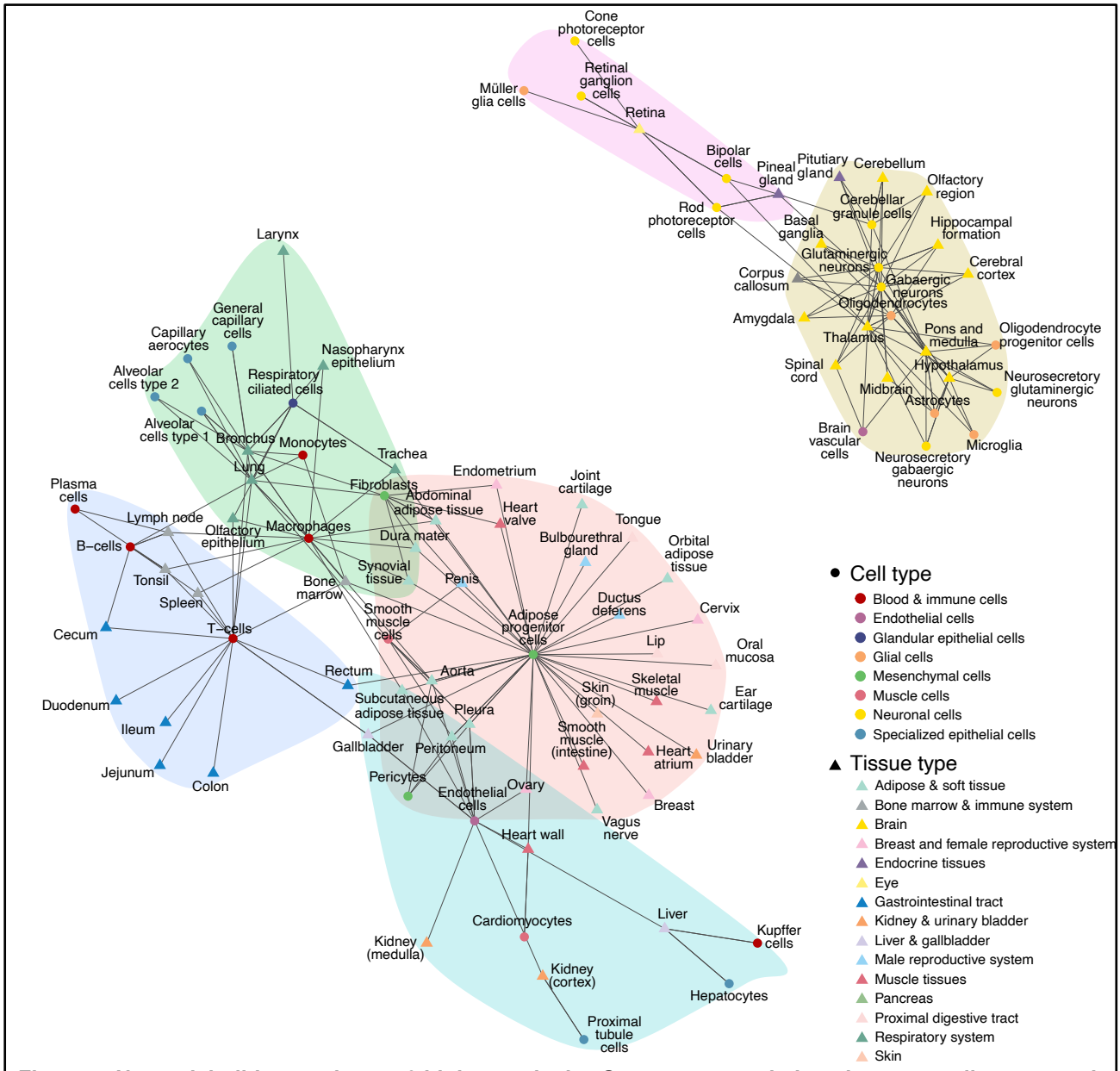

Figure 7. Network build upon the top 3 highest pairwise Spearman correlations between cells types and tissue types based on enriched genes. All available tissue types of the bulk RNA atlas were included for this comparison.

with the annotations of genes based on the bulk data. Firstly, there are more genes detected in the single-cell dataset. Secondly, there is a higher amount of tissue enhanced genes in single-cell data, compared to bulk data. In the bulk data, there is a predominant number of genes with low tissue specificity.

I also compared the Tau scores calculated for each gene based on the two different datasets. The histograms in **Figure 6C** highlight that the single-cell dataset computes for higher number of high Tau score genes than the bulk dataset. This argues that annotating the specificity of genes based on their expression in single cells provides more information about their specificity.

Next, I aimed to assess the similarities between cell types and tissue types. A hypergeometric test based on matching elevated genes between bulk and single-cell data was performed (**Figure 6B**). This test serves as a control of the data to confirm both correct annotation and sampling of the single-cell data. We can observe that cell types can be traced back to their tissue of origin.

However, a few cell types show a significant overlap of enriched genes with other tissues, such as the brain vascular cells with adipose tissue, ependymal cells with the lung, or various kidney cells with the liver tissue and liver cells with the kidney tissue. I further investigated some of these relationships through the atlas to corroborate them to be originating from genes involved in shared molecular processes of two tissues (**Figure 9A**).

A similar test specific to brain tissues only was performed (**Figure S7**). The result of this test provides into the populations of neurons found in each brain region. Notably, glutaminergic and gabaergic neurons have significantly shared elevated genes between the amygdala, basal ganglia, cerebral cortex, hippocampal formation, and the olfactory region, however not in the cerebellum, corpus collosum, hypothalamus, midbrain, or pons and medulla. Medium spiny neurons share elevated genes with the basal ganglia, the cerebellar cells with the cerebellum, and neurosecretory neurons with the hypothalamus and pons and medulla, the pituitary gland, and basal ganglia. The pineal gland and retina tissues seem to have also similar cell makeup due to, them coinciding significantly with the same cell types.

Lastly, I aimed to evaluate the question of how well the single-cell transcriptomic dataset represented the whole bulk tissue dataset. For this purpose, I calculated the pairwise Spearman correlations between cell types and tissue types and visualized them in a network plot as seen in **Figure 7**. Similarly, as in the hypergeometric test, the result demonstrated that cells correlate the most to the tissues, in which they are present. For example, immune cells correlate highly with the lymph node and spleen, proximal tubule cells correlate with the cortex region of the kidney, or hepatocytes and Kupffer cells correlate with the liver. Also, immune cells exhibited a high correlation with tissues having mucosal surfaces like the respiratory or digestive tract. Adipose progenitor cells locate themselves in the center of connective tissues like the skin, muscle tissue, breasts, and other soft tissues, in addition to adipose tissues.

Comparison to human single-cell data

To compare the human and the pig single-cell datasets, given the differences in detected cells and cell type annotation, I had to create a new consensus nomenclature between both tissue types (**Figure S8**). Based on the consensus names, I created a new comparison dataset for both pig and human single-cell data, containing only orthologous genes (N = 16,715) shared between both species. With this in place, similar to the previous section, I classified all protein-coding genes based on their specificity (**Figure 8A**). The number of genes assigned to each category is comparably similar.

With the annotation in place, I next aimed to compare the similarities between cell types through this control for correct cell type labelling. I conducted thus a more detailed comparison of each consensus cell type by performing a hypergeometric test based on shared elevated genes (**Figure 8B**). We see that every matching cell type shares significant overlap in matching enriched genes, as expected. Additionally, cell types undergoing similar processes share enriched genes as well. For example, microglia share overlap with immune cells like macrophages, Kupffer cells, and monocytes.

To compare the overall expression profile of the pig and human datasets, I visualized them in a UMAP plot (**Figure 8C**). In this plot, we can observe that mostly matching cell types do cluster

together. The only outlier is the intestinal epithelial cells. The pig intestinal epithelial cells cluster together with blood and immune cells instead.`

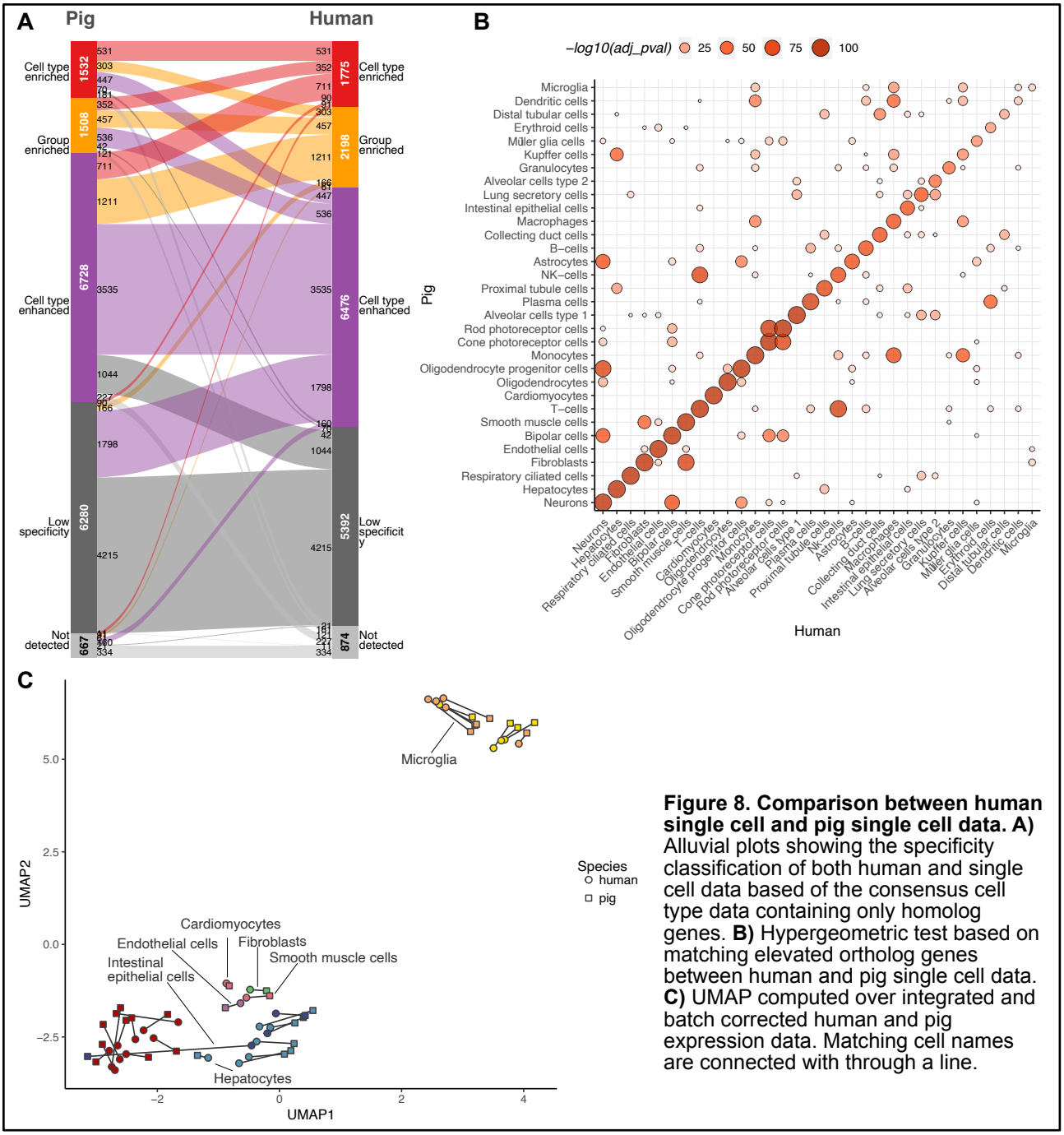

Figure 8. Comparison between human single cell and pig single cell data. A) Alluvial plots showing the specificity classification of both human and single cell data based of the consensus cell type data containing only homolog genes. **B)** Hypergeometric test based on matching elevated ortholog genes between human and pig single cell data. **C)** UMAP computed over integrated and batch corrected human and pig expression data. Matching cell names are connected with through a line.

Discussion

Identification of cell types

The pig single-cell atlas is built upon the single-cell transcriptomic libraries from 24 samples, encompassing 11 tissues and 9 brain regions. The tissue sections in the dataset (**Figure 1A**) originate predominantly from functional organs, except for the adipose tissues, which are connective tissue, as well as the PBMC. These sections are valuable for studies on cardiovascular disease, diabetes, metabolism, infectious and airborne diseases, cystic fibrosis, and a variety of cancers among other things.

The organ sections of the intestine, kidney, liver, and lung would be expected to be predominantly composed of epithelial tissues featuring their organ specific parenchymal or specialized epithelial cells. While this holds true for the kidney, liver, and lung sections, it is not the case for the intestine (**Figures 3, S1, S5**).

Consistent with a previous human kidney atlas published,[26] the kidney was predominantly populated by proximal tubule cells. Other cell types such as podocytes, loop of Henle cells, distal tubule cells, and collecting duct cells are equally detected in kidney atlases. Missing in this atlas are however glomerular parietal cells, which due to their usually low cell population and the low cluster definition in the pig sample might have not been able to form an independent cluster. To note, renal interstitial cells, are a mixture of mesenchymal cells in the kidney's stroma.

Similarly, for the cell annotation of the liver, cell types are consistent with what was identified in a human liver atlas.[27] The tissue is predominantly composed of hepatocytes. As reported in the human liver atlas, there is a predominant presence of Kupffer cells, T cells, and other immune cells. Two populations of Kupffer cells were detected: potentially inflammatory and non-inflammatory Kupffer cells. Unfortunately, cholangiocytes were not detected, although low expression of cholangiocyte markers EPCAM and ONECUT1 in the hepatocyte clusters of the liver snRNA-seq sample suggest that they were present in the sample, only the independent clustering formation for this cell type was not successful.

The scRNA-seq sample of the lung included an unexpectedly high number of immune cells, which would hint towards a flawed digestion process after sectioning. Only 98 non-immune cells (labelled as lung epithelial cells) from 10,906 cells were identified. The resulting cell population of the snRNA-seq lung sample on the other hand was successful and is comparable to a previous human lung cell atlas[28] with regards to the cell types identified. As expected, alveoli epithelial cells alveolar type 1 and type 2 (AT1 and AT2) were identified, as well as respiratory ciliated cells of the airway epithelia. The cell type labelled as respiratory secretory cells includes airway mucus-secreting epithelial cells such as club cells or goblet cells that did not cluster separately. As for the human,[28] two main capillary cell types were identified: general capillary cells and the newly discovered[28] capillary aerocytes.

Like the lung scRNA-seq sample, the intestine sample seems to have failed the digestion process. Only 227 cells from 11,767 intestinal cells are non-immune. They were labelled as intestinal epithelial cells and endothelial cells. Unfortunately, due to the low number of cells, no higher resolution was obtainable. Additionally, 54 enteric glial and enteroendocrine cells were detected, however, they were in a single cluster and could not be told apart. The cluster data was thus not included in the final expression dataset.

The heart is the only tissue in the atlas' sample set, that is expected to be predominantly muscle tissue. This was the case; the heart single-cell library was composed predominantly of cardiomyocytes. The atrial cardiomyocytes marker MYL4 was not expressed in cardiomyocytes and marker NPPA only at low levels (7.4 nTPM), suggesting that these are only ventricular cardiomyocytes and that the heart atrium was not included in the tissue section. Aside from this,

the cell population is like the one described in the human heart single-cell atlas[29], albeit the heart library includes a relatively low number of cells (N = 3,323).

Connective tissue is only represented by the two adipose tissue samples: visceral adipose (adipose-V) and subcutaneous adipose (adipose-S). Both samples are scRNA-seq samples, which consequently yielded no adipocyte to be detected. Adipocytes store fat, which is more buoyant than water, and thus escapes single-cell sample preparation. Adipocytes are thus better detectable using snRNA-seq, however, I had no access to a pig single nuclei adipose sample. Aside from missing adipocytes, both adipose tissues are consistent with human adipose single-cell studies.[30] As in the human adipose atlas, visceral adipose contains mesothelial cells and a higher diversity of immune cells in comparison to subcutaneous adipose. Also as described in the human adipose cell atlas, adipocyte progenitors, fibroblasts and mesenchymal stem cells are very closely related, and are difficult to tell apart due to their similarity.[30] They are here labeled as adipose progenitors.

The spleen is expected to be mostly populated out of a variety of immune cells, as it is part of the lymphatic system responsible for blood filtration. As expected, it includes a wide variety of immune cells. However, there were a few endothelial cells and muscle cells detected as well in the snRNAseq sample. The single nuclei sample identified additionally endothelial cells and smooth muscle cells which could originate from blood vessels in the section.

PBMC is known to be populated by lymphocytes (T-cells, B-cells, NK-cells), monocytes, and dendritic cells. This is consistent with what I have identified in the single-cell library. Additionally, very few megakaryocytes and platelets were detected, which are not supposed to be found in the PBMC. However, as they are a minor component of the sample, it might be due to minor contamination during the isolation.

The 10 brain samples cover together a significant portion of the brain (**Figure 1**). The atlas includes data from all four lobes of the cerebral cortex, the cerebellum, and the hypothalamus in both single-cell and single nuclei. These together with the single-cell data from the basal ganglia, thalamus, hippocampus, and pons cover a large amount of the brain. Included are in addition three of the four circumventricular organs: subformical organ, the vascular organ of lamina terminalis (VOLT), and the area postrema. These are brain regions that are in contact with the blood and enable exchange between the central nervous system and the circulating blood and thus have endocrine function.[31]

Cell annotation for nerve tissues has been a technical and conceptual challenge in the field.[32] Annotation can vary based on neuron morphology or the type of neurotransmitter produced. Neurons in retina single-cell libraries however have been annotated mostly based on their morphology. I also took this approach and identified: rod cells, cone cells, ganglion cells, and bipolar cells. Other retina atlases identify additionally amacrine cells and horizontal cells,[33,34] which were not identified in the pig libraries. These cells may have clustered however inside the ganglion cells clusters, since these clusters are expressing genes like TFAP2B, C1QL2, or GAD1, which are known markers for amacrine or horizontal cells in the retina.[33,34] Overall, the retina samples yielded poor cluster definitions (**Figure S2**), which may have hindered the proper identification of these cells.

For the brain tissues, I decided to take a mixed approach. I aimed to define clusters of neurons by morphology if this was possible through transcriptomic data. Otherwise, I would define them primarily on if they produced predominantly GABA or glutamine as a neurotransmitter as GABAergic or glutaminergic. If they did not express GABA or glutamine, then they would be defined by any other neurotransmitter they expressed, such as cholinergic, serotinergic, or dopaminergic. Additionally, due to the presence of the circumventricular organs, I labelled hormone-secreting neurons as neurosecretory. By morphology, I identified cerebellar granule, Purkinje and stellate cells, and medium spiny neurons.

Labeling neurons by neurotransmitter however proved to be challenging. The data showed often poor cluster definition, which is why re-clustering of the data was performed, to obtain the desired neuron cluster resolution. Additionally, it is normal for neurons to express simultaneously both GABA and glutamine or combinations of other neurotransmitters. I settled on labeling the neuron based on the highest expressed neurotransmitter, however, this approach is not entirely reproducible and thus not ideal. Better suited annotation formats could be adopted from the single-cell brain atlases such as the mouse brain atlas by Zeisel, et al.[35] Here, neuron clusters are given rather a code symbol as a label and annotated the (multiple) neurotransmitters as tags. Morphological information can be added as well. This approach might be however too complex and detailed for a multi-tissue single-cell atlas.

To conclude on the cell type identification section, cell types in every organ were labelled and compared based on the available human single-cell atlases of every organ. For most organs, the labelling was consistent, only the intestine sample, showed technical difficulties during tissue digestion. Recurrent problems in some samples however were poor cluster definition and low cell count numbers in some transcript libraries. These sometimes hindered identifying some expected cell types in the samples. The method of annotating neurons could be still improved to be more reproducible.

A multi-organ cell-type transcriptome map of the pig

Overall, the pseudo-bulk transcriptome data on 66 cell types did yield comprehensible cell type expression profiles (**Figure 2**). The cell type clustering in **Figure 2C**, demonstrates mostly comprehensible cell type relationships, as annotated in the figure. Additionally, single-cell data presents itself as a valuable complement to the bulk data, since genes are more specific to cell types than to tissues (**Figure 6A, C**), which can aid methods like gene function annotation through gene clustering or generally give a more detailed insight of shared molecular processes between cell types. **Figure 6B** shows that single-cell is indeed consistent with what was observed in the bulk tissue pig atlas.

Figure 6B highlights additional interesting relationships between them. Kidney and Liver cells share enriched genes, due to their known shared task in detoxification. They coincide in the production of organic cation transport proteins, such as SLC22A1 (**Figure 9A**). Additionally, mucus-secreting cells of the lung share enriched genes with the intestine; or ependymal cells in the brain carry cilia like the respiratory ciliated cells in the lung. **Figure S7** highlights some relationships between brain cells with brain regions. Medium spiny neurons are highly populated in the basal ganglia. The corpus collosum is predominantly populated with oligodendrocytes and not neurons, and the

pinacocytes in the pineal gland are photoreceptors cells expressing melatonin similar to cells in the retina.[36]

Figure 8B suggests correct labelling of cell types since matching pig and human cells indeed show a significant amount of matching elevated genes. However, intestinal epithelial cells clustering with myeloid cells in **Figure 2C** and **Figure 8C** highlights some issues of the dataset. Aside from the flawed intestine tissue digestion discussed in the previous section, it seems that there is significant ambient RNA present in the transcript data, which caused them to cluster together. Ambient RNA is understood as RNA residing outside of the cells, which can then be captured in solution together with the cell or nuclei in a droplet and can be labelled and amplified with the rest of the intracellular or intranuclear transcripts.[37] There could be similar to the intestine sample, a high degree of ambient RNA in other samples. Suspects of this are for example also kidney and retina, both of which equally showed low cluster resolution and their cell types of clusters together in **Figure 2**.

Figure 8B gives further insight into what cells may have high ambient RNA contamination. For example, the expression data of pig astrocytes overlaps highly with neurons. In human astrocytes, this is not the case since the astrocytes do not overlap as much with neurons. Similar can be said with hepatocytes and Kupffer cells. There is no overlap of human Kupffer cells with pig hepatocytes, however, there is a large overlap of pig Kupffer cells with human hepatocytes. This is also observed for pig plasma cells with erythroid cells and pig intestinal epithelial cells with T cells.

A further issue with the dataset is that despite the similarities and consistency across methods, the single-cell atlas is not able to give a whole-body cell transcript picture of the pig. As mentioned, the library is primarily composed of functional organs, and disregards connective tissue and muscle tissue. Adipose is the unique connective tissue in the dataset and this is potentially why adipose progenitor cells correlate the highest with multiple tissues (**Figure 7**). Cells rather expected to be there, include fibroblasts, smooth muscle cells, or endothelial cells, but in the single-cell dataset, they were usually detected as part of vascular tissue and not connective tissue. The single-cell dataset thus has rather an incomplete picture of those cell types that are predominant connective tissues.

A navigable framework for single-cell atlas exploration

Aside from going through the processing and labeling of data to generate a single-cell, I had the objective of creating a navigable framework for the atlas by annotating all protein-coding genes with cell type specificity categories and a Tau score, similarly as done previously by the Human Protein Atlas.[9,16] This framework should allow for efficient explorations of the genes in the atlas while maintaining a holistic view of the gene expression across cell types.

The practicality of this approach can be exemplified in the network plot in **Figure 5.** Through this framework, it is possible to swiftly find cell type markers by searching for cell type enriched genes. Similarly, it can enable to find shared enriched genes between different cell types, which would hint toward shared molecular processes. The other way around is also true. If a researcher is looking to validate the involvement of a gene in a certain process across different cell types, this can be easily done by these categories, independent from the absolute nTPM expression values. This allows streamlining of any kind of research involving the pig as a model system. Multiple kinds of research areas can consequently benefit from this by facilitating hypothesis generation. From for example

research on determining entry points of zoonotic diseases (**Figure 9B**) to determining novel disease markers to researching into creating gene function networks in cells (**Figure 9C**).

Eventually, a visualization of gene expression of a gene for this single-cell atlas could be presented in **Figure 9**. In a single plot, one can acquire information on the expression of a gene in a cell type but also specifically in what tissue this is expressed and if there are any changes in the expression of this gene across tissues in the same cell type.

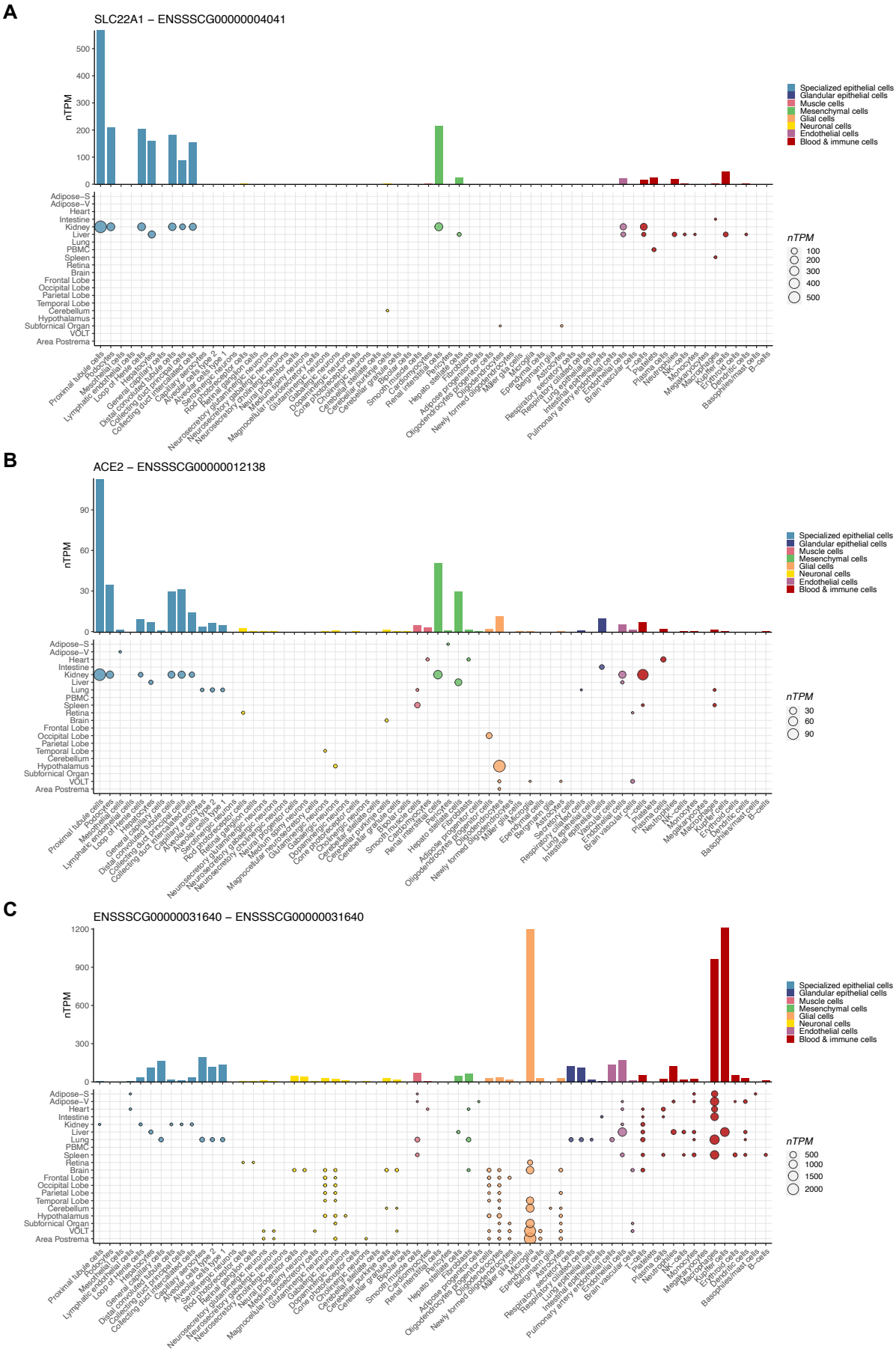

Figure 9. Examples of use cases and presentation of the pig single cell transcriptomic atlas. A) Genes expressed in shared tissues. SLC22A1, a cation transport protein, expressed in tissues of the lung and the liver. **B)** Mapping of viral entry points of zoonotic disease, by the example of the ACE2 receptor, entry point of the SARS-CoV-2 virus. **C)** Discovery of cell type specific genes exemplified by a group enriched gene in microglia, macrophages and Kupffer cells.

Future work

Throughout the discussion, several aspects were identified that could be improved upon in future work. To summarise, one key issue is the presence of ambient RNA contaminating a portion of the identified cell types. Ambient RNA and low sample cell count may yield consequently poor cluster resolution and miss the identification of important cell types within tissues. Additionally, the tissues available for the atlas were biased towards being functional organs, which in turn does not give a complete picture of the cell types ubiquitous to connective and muscle tissue, such as fibroblasts, endothelial cells, and smooth muscle cells.

As a short-term goal for this atlas, I would suggest for future work for this atlas, to employ tools that remove ambient RNA contamination from the samples, such as SoupX[37] or DecontX[38], and assess how this affects the overall atlas. Although this process would require repeating the entire labeling procedure, it is crucial to establish a higher cluster definition. Moreover, adjusting the framework of neuron labelling, to permit the labels of multiple neurotransmitters should be considered. This might involve creating a separate atlas for the pig brain only. This approach would otherwise yield considerably more cell types for the brain compared to other tissues.

Furthermore, several investigations can be conducted with the dataset. Gene clustering methods based on single-cell data could be employed to assign gene function annotation to genes, providing a useful complement to the atlas. Karlsson et al.[16] performed such clustering in the pig based on bulk data. However, as I reported here, there is more specificity information at the single-cell level, and I would thus expect a better resolution in the gene function annotation when using single-cell data. With such an annotation, pathway analysis can be performed instead of analysing independent genes. I would suggest using these gene function annotations to detect “enriched pathways” in cell types instead of enriched genes. This would give more informative results, compared to enriched genes. Similarly, inter-species comparisons such as human and pig could be performed based on differences in enriched pathways. Such a comparison would yield more meaningful and robust results, compared to determining differences based on a single gene.

I reported in this atlas an integration of both single-cell and single-nuclei datasets. It would be interesting to further investigate the differences between scRNA-seq and snRNA-seq cell transcriptomes and investigate on potential biases of every method. Certain cell types, such as hepatocytes, various immune cells, oligodendrocytes, and neurons, were detected using both methods, making them suitable for comparative analysis. Understanding the quantitative differences beyond the expected variations in mature transcripts, mitochondrial RNA, and ribosomal RNA between the two methods would be valuable. Gaedcke et al.[39] compared snRNA-seq to scRNA-seq transcription profiles of proximal tubule cells of the mouse liver, and identified through gene ontology enrichment analysis that scRNA-seq was more prone to identifying genes related to inflammation processes, while snRNA-seq cells, were prone to identifying genes related to extracellular matrix organization, morphogenesis, and cell cycle related processes. It would be valuable to assess if such relationships are maintained across cell types. So far, we see in Figure 2A higher differences between methods for immune cells and hepatocytes, compared to neurons. I do need to stress, that the dataset may not be ideal for this analysis, as the data comes from

different organisms and were sampled at different ages (three-month-old pigs vs. six-month-old pigs). Nevertheless, it can serve as a starting point to assess this question.

On the other hand, a long-term goal would be to try to counteract the bias towards functional organs and complete the picture, particularly for smooth muscle cells, fibroblasts, and endothelial cells. There are diseases involving failure of muscle or connective tissues studied in pigs, that would benefit from this data, such as research in muscular dystrophy or osteosarcomas.[17] Additionally, considering the important role of pigs in xenotransplantation[17] research, establishing a cell-type atlas, encompassing tissues from the whole body would be valuable. Additionally, the atlas would benefit, if more than only one organism would be used per section to reduce bias.

Finally, as mentioned, this atlas will complement the bulk tissue atlas of the pig available at www.rnaatlas.org. In the future, the goal is to extend this atlas to include both bulk and single-cell level for various mammalian species, establishing ultimately the Mammalian RNA Atlas.

Ethical reflection

In this master thesis, I report the process involved of generating a single-cell atlas of the pig. The researchers involved in producing the raw data did report approval from the responsible ethical committees and adhered to their applicable national and institutional animal use and welfare guidelines.

The creation of an easily accessible and comprehensive single-cell atlas of the pig serves to reduce the number of animals used in scientific research. By providing a reliable database, this atlas can facilitate hypothesis generation and potentially eliminate the need for unnecessary experimentation with pigs. The atlas promotes more efficient and informed use of animals by ensuring that hypotheses are well-supported before conducting experiments.

Additionally, the research also features that at a cellular level, there are few differences between pigs and humans. Tissues and organs of both organisms are composed of the same cell types formed of equal building blocks. Pigs exhibit complex social and cognitive capacities.[40] As mammals, both pigs and humans share the same biological necessities for well-being. By highlighting the similarities between pig and human at a cellular level, might argument for improved standards of animal use and animal welfare.

Acknowledgements

I would like to acknowledge the following people for their support during the degree project:

I would like to thank my supervisor Linn Fagerberg for her guidance and support throughout the project. I am grateful to her for allowing me to collaborate with the Human Protein Atlas for my degree project and providing me with insightful advice on how to steer the whole project. I appreciate her confidence in me, allowing for very independent work and am also grateful for her swift assistance whenever I faced last minute issues.

I would like to thank Mengnan Shi for introducing me to the single-cell pipeline analysis and helping me out when I had any single-cell data processing related question. Her assistance was key for my data processing pipeline.

I also would like to acknowledge Max Karlsson, for showing how to use R to make great plots and introducing me to the bulk data analysis pipeline. Although our exchange was before starting my master thesis project, without his guidance, this project would have not been of the same quality.

I am grateful to Jan Mulder and Evelina Sjöstedt, for their helpful discussions on cell type labeling and reasoning on my results.

References

1. Ramón y Cajal, S. *Histologie du système nerveux de l'homme et des vertébrés*. (1909).
2. Hershey, B. A. D. & Chase, M. Independent functions of viral protein and nucleic acid in growth of bacteriophage. *Journal of General Physiology* **36**, 39–56 (1952).
3. Crick, F. On Protein Synthesis. *The Symposia of the Society for Experimental Biology* 138–163 (1958).
4. Venter, J. C. *et al.* The Sequence of the Human Genome. *Science (1979)* **291**, 1304–1351 (2001).
5. International Human Genome Sequencing Consortium *et al.* Initial sequencing and analysis of the human genome. *Nature* **409**, (2001).
6. Brenner, S. *Sydney Brenner - Nobel Lecture: Nature's Gift to Science*. (2002).
7. Tang, F. *et al.* mRNA-Seq whole-transcriptome analysis of a single cell. *Nat Methods* **6**, 377–382 (2009).
8. Islam, S. *et al.* Characterization of the single-cell transcriptional landscape by highly multiplex RNA-seq. *Genome Res* **21**, 1160–1167 (2011).
9. Karlsson, M. *et al. A single-cell type transcriptomics map of human tissues*. *Sci. Adv* vol. 7 www.proteinatlas.org (2021).
10. Jones, R. C. *et al.* The Tabula Sapiens: A multiple-organ, single-cell transcriptomic atlas of humans. *Science (1979)* **376**, (2022).
11. Vandereyken, K., Sifrim, A., Thienpont, B. & Voet, T. Methods and applications for single-cell and spatial multi-omics. *Nature Reviews Genetics* Preprint at https://doi.org/10.1038/s41576-023-00580-2 (2023).
12. Adil, A., Kumar, V., Jan, A. T. & Asger, M. Single-Cell Transcriptomics: Current Methods and Challenges in Data Acquisition and Analysis. *Frontiers in Neuroscience* vol. 15 Preprint at https://doi.org/10.3389/fnins.2021.591122 (2021).
13. Dai, X. & Shen, L. Advances and Trends in Omics Technology Development. *Frontiers in Medicine* vol. 9 Preprint at https://doi.org/10.3389/fmed.2022.911861 (2022).
14. Rood, J. E., Maartens, A., Hupalowska, A., Teichmann, S. A. & Regev, A. Impact of the Human Cell Atlas on medicine. *Nat Med* **28**, 2486–2496 (2022).
15. Chen, D. *et al.* Single cell atlas for 11 non-model mammals, reptiles and birds. *Nat Commun* **12**, (2021).
16. Karlsson, M. *et al.* Genome-wide annotation of protein-coding genes in pig. *BMC Biol* **20**, (2022).
17. Lunney, J. K. *et al. Importance of the pig as a human biomedical model*. *Sci. Transl. Med* vol. 13 https://www.science.org (2021).
18. Gutierrez, K., Dicks, N., Glanzner, W. G., Agellon, L. B. & Bordignon, V. Efficacy of the porcine species in biomedical research. *Front Genet* **6**, (2015).
19. Wang, F. *et al.* Endothelial cell heterogeneity and microglia regulons revealed by a pig cell landscape at single-cell level. *Nat Commun* **13**, (2022).
20. Zhu, J. *et al.* Single-cell atlas of domestic pig cerebral cortex and hypothalamus. *Sci Bull (Beijing)* **66**, 1448–1461 (2021).
21. Zhang, L. *et al.* A high-resolution cell atlas of the domestic pig lung and an online platform for exploring lung single-cell data. *Journal of Genetics and Genomics* **48**, 411–425 (2021).
22. Warr, A. *et al.* An improved pig reference genome sequence to enable pig genetics and genomics research. *Gigascience* **9**, (2020).
23. Korsunsky, I. *et al.* Fast, sensitive and accurate integration of single-cell data with Harmony. *Nat Methods* **16**, 1289–1296 (2019).
24. Robinson, M. D. & Oshlack, A. *A scaling normalization method for differential expression analysis of RNA-seq data*. http://genomebiology.com/2010/11/3/R25 (2010).

25. Yanai, I. *et al.* Genome-wide midrange transcription profiles reveal expression level relationships in human tissue specification. *Bioinformatics* **21**, 650–659 (2005).
26. Liao, J. *et al.* Single-cell RNA sequencing of human kidney. *Sci Data* **7**, (2020).
27. MacParland, S. A. *et al.* Single cell RNA sequencing of human liver reveals distinct intrahepatic macrophage populations. *Nat Commun* **9**, (2018).
28. Travaglini, K. J. *et al.* A molecular cell atlas of the human lung from single-cell RNA sequencing. *Nature* **587**, 619–625 (2020).
29. Litviňuková, M. *et al.* Cells of the adult human heart. *Nature* **588**, 466–472 (2020).
30. Norreen-Thorsen, M. *et al.* A human adipose tissue cell-type transcriptome atlas. *Cell Rep* **40**, (2022).
31. Ganong, W. F. Circumventricular organs: Definition and role in the regulation of endocrine and autonomic function. in *Clinical and Experimental Pharmacology and Physiology* vol. 27 422–427 (2000).
32. Zeng, H. & Sanes, J. R. Neuronal cell-type classification: Challenges, opportunities and the path forward. *Nature Reviews Neuroscience* vol. 18 530–546 Preprint at https://doi.org/10.1038/nrn.2017.85 (2017).
33. Liang, Q. *et al.* A multi-omics atlas of the human retina at single-cell resolution. *Cell Genomics* 100298 (2023) doi:10.1016/j.xgen.2023.100298.
34. Menon, M. *et al.* Single-cell transcriptomic atlas of the human retina identifies cell types associated with age-related macular degeneration. *Nat Commun* **10**, (2019).
35. Zeisel, A. *et al.* Molecular Architecture of the Mouse Nervous System. *Cell* **174**, 999-1014.e22 (2018).
36. Pandi-Perumal, S. R. *et al.* Melatonin: Nature's most versatile biological signal? *FEBS Journal* vol. 273 2813–2838 Preprint at https://doi.org/10.1111/j.1742-4658.2006.05322.x (2006).
37. Young, M. D. & Behjati, S. SoupX removes ambient RNA contamination from droplet-based single-cell RNA sequencing data. *Gigascience* **9**, (2020).
38. Yang, S. *et al.* Decontamination of ambient RNA in single-cell RNA-seq with DecontX. *Genome Biol* **21**, (2020).
39. Gaedcke, S. *et al.* Single cell versus single nucleus: Transcriptome differences in the murine kidney after ischemia-reperfusion injury. *Am J Physiol Renal Physiol* **323**, F171–F181 (2022).
40. Warr, A. *et al.* An improved pig reference genome sequence to enable pig genetics and genomics research. *Gigascience* **9**, (2020).

Supplementary Figures

Figures bellow.

Figure S1 & S2. Data presentation of the 24 samples individually. For every sample, a UMAP plot, a dendrogram and a cell count barplot was computed. The UMAP plot, as calculated by the scanpy preprocessing pipeline and labelled with the cluster names. The dendrogram shows the relationship between the assigned cell types inside the sample. The bar plot pictures the number of cells detected per cell type inside a sample.

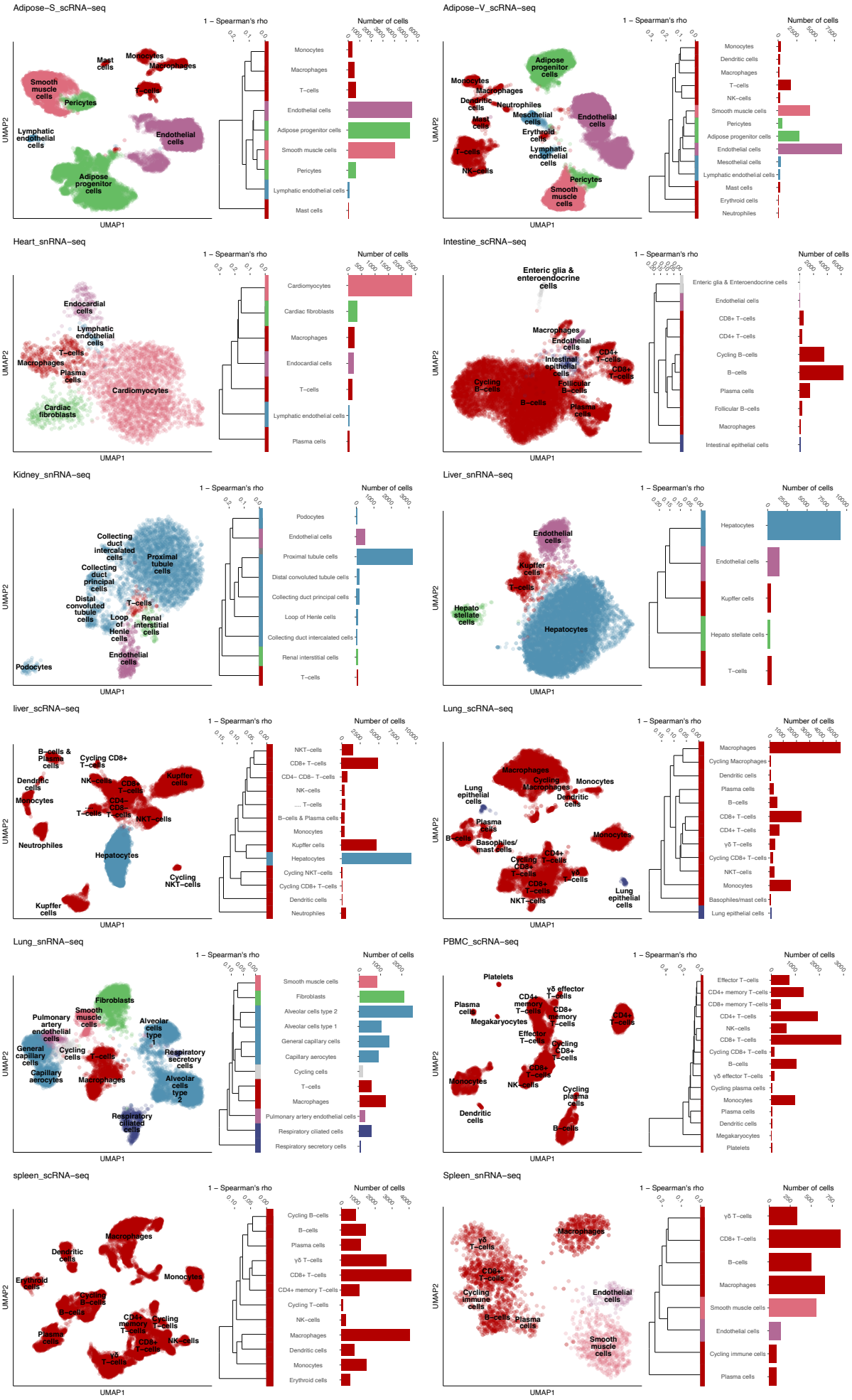
Adipose−S_scRNA−seq
1 − Spearman's rho
Number of cells
Monocytes
Macrophages
T−cells
Endothelial cells
Adipose progenitor cells
Smooth muscle cells
Pericytes
Lymphatic endothelial cells
Mast cells
Mast cells
Monocytes
Macrophages
Smooth muscle cells
Pericytes
T−cells
Lymphatic endothelial cells
Endothelial cells
Adipose progenitor cells
UMAP1
UMAP2
Adipose−V_scRNA−seq
1 − Spearman's rho
Number of cells
Monocytes
Dendritic cells
Macrophages
T−cells
NK−cells
Smooth muscle cells
Pericytes
Adipose progenitor cells
Endothelial cells
Mesothelial cells
Lymphatic endothelial cells
Mast cells
Erythroid cells
Neutrophiles
Adipose progenitor cells
Monocytes
Macrophages
Dendritic cells
Neutrophiles
Mesothelial cells
Mast cells
Erythroid cells
Endothelial cells
T−cells
Lymphatic endothelial cells
NK−cells
Pericytes
Smooth muscle cells
UMAP1
UMAP2
Heart_snRNA−seq
1 − Spearman's rho
Number of cells
Cardiomyocytes
Cardiac fibroblasts
Macrophages
Endocardial cells
T−cells
Lymphatic endothelial cells
Plasma cells
Endocardial cells
Lymphatic endothelial cells
T−cells
Macrophages
Plasma cells
Cardiomyocytes
Cardiac fibroblasts
UMAP1
UMAP2
Intestine_scRNA−seq
1 − Spearman's rho
Number of cells
Enteric glia & Enteroendocrine cells
Endothelial cells
CD8+ T−cells
CD4+ T−cells
Cycling B−cells
B−cells
Plasma cells
Follicular B−cells
Macrophages
Intestinal epithelial cells
Enteric glia & enteroendocrine cells
Macrophages
Endothelial cells
Intestinal epithelial cells
CD4+ T−cells
CD8+ T−cells
Cycling B−cells
Follicular B−cells
B−cells
Plasma cells
UMAP1
UMAP2
Kidney_snRNA−seq
1 − Spearman's rho
Number of cells
Podocytes
Endothelial cells
Proximal tubule cells
Distal convoluted tubule cells
Collecting duct principal cells
Loop of Henle cells
Collecting duct intercalated cells
Renal interstitial cells
T−cells
Collecting duct intercalated cells
Collecting duct principal cells
Proximal tubule cells
Distal convoluted tubule cells
T−cells
Loop of Henle cells
Renal interstitial cells
Endothelial cells
Podocytes
UMAP1
UMAP2
Liver_snRNA−seq
1 − Spearman's rho
Number of cells
Hepatocytes
Endothelial cells
Kupffer cells
Hepato stellate cells
T−cells
Endothelial cells
Kupffer cells
T−cells
Hepato stellate cells
Hepatocytes
UMAP1
UMAP2
liver_scRNA−seq
1 − Spearman's rho
Number of cells
NKT−cells
CD8+ T−cells
CD4− CD8− T−cells
NK−cells
.... T−cells
B−cells & Plasma cells
Monocytes
Kupffer cells
Hepatocytes
Cycling NKT−cells
Cycling CD8+ T−cells
Dendritic cells
Neutrophiles
B−cells & Plasma cells
Cycling CD8+ T−cells
Dendritic cells
NK−cells
CD8+ T−cells
Monocytes
CD4− CD8− T−cells
T−cells
NKT−cells
Kupffer cells
Neutrophiles
Hepatocytes
Cycling NKT−cells
Kupffer cells
UMAP1
UMAP2
Lung_scRNA−seq
1 − Spearman's rho
Number of cells
Macrophages
Cycling Macrophages
Dendritic cells
Plasma cells
B−cells
CD8+ T−cells
CD4+ T−cells
γδ T−cells
Cycling CD8+ T−cells
NKT−cells
Monocytes
Basophiles/mast cells
Lung epithelial cells
Macrophages
Cycling Macrophages
Monocytes
Lung epithelial cells
Dendritic cells
Plasma cells
B−cells
Basophiles/ mast cells
Monocytes
CD4+ T−cells
Cycling CD8+ T−cells
γδ T−cells
CD8+ T−cells
NKT−cells
Lung epithelial cells
UMAP1
UMAP2
Lung_snRNA−seq
1 − Spearman's rho
Number of cells
Smooth muscle cells
Fibroblasts
Alveolar cells type 2
Alveolar cells type 1
General capillary cells
Capillary aerocytes
Cycling cells
T−cells
Macrophages
Pulmonary artery endothelial cells
Respiratory ciliated cells
Respiratory secretory cells
Fibroblasts
Smooth muscle cells
Pulmonary artery endothelial cells
Alveolar cells type 1
General capillary cells
Cycling cells
T−cells
Respiratory secretory cells
Capillary aerocytes
Macrophages
Alveolar cells type 2
Respiratory ciliated cells
UMAP1
UMAP2
PBMC_scRNA−seq
1 − Spearman's rho
Number of cells
Effector T−cells
CD4+ memory T−cells
CD8+ memory T−cells
CD4+ T−cells
NK−cells
CD8+ T−cells
Cycling CD8+ T−cells
B−cells
γδ effector T−cells
Cycling plasma cells
Monocytes
Plasma cells
Dendritic cells
Megakaryocytes
Platelets
Platelets
γδ effector T−cells
Plasma cells
CD4+ memory T−cells
CD8+ memory T−cells
CD4+ T−cells
Megakaryocytes
Effector T−cells
Cycling CD8+ T−cells
CD8+ T−cells
Monocytes
NK−cells
Cycling plasma cells
Dendritic cells
B−cells
UMAP1
UMAP2
spleen_scRNA−seq
1 − Spearman's rho
Number of cells
Cycling B−cells
B−cells
Plasma cells
γδ T−cells
CD8+ T−cells
CD4+ memory T−cells
Cycling T−cells
NK−cells
Macrophages
Dendritic cells
Monocytes
Erythroid cells
Macrophages
Dendritic cells
Monocytes
Erythroid cells
Cycling B−cells
B−cells
Plasma cells
CD4+ memory T−cells
Cycling T−cells
CD8+ T−cells
γδ T−cells
NK−cells
UMAP1
UMAP2
Spleen_snRNA−seq
1 − Spearman's rho
Number of cells
γδ T−cells
CD8+ T−cells
B−cells
Macrophages
Smooth muscle cells
Endothelial cells
Cycling immune cells
Plasma cells
Macrophages
γδ T−cells
CD8+ T−cells
Cycling immune cells
B−cells
Plasma cells
Endothelial cells
Smooth muscle cells
UMAP1
UMAP2

retina_scRNA−seq

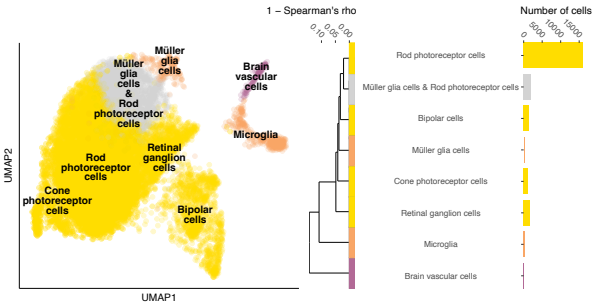

Retina_snRNA−seq

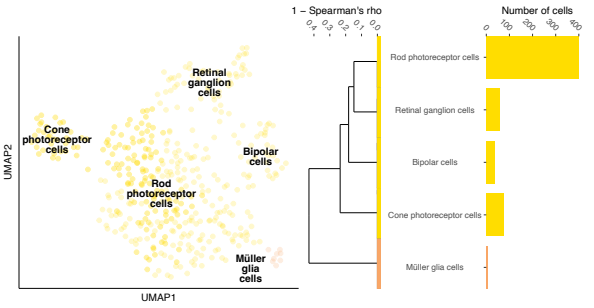

brain_scRNA−seq

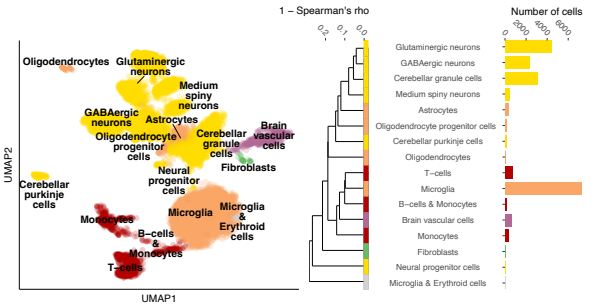

Frontal lobe_snRNA−seq

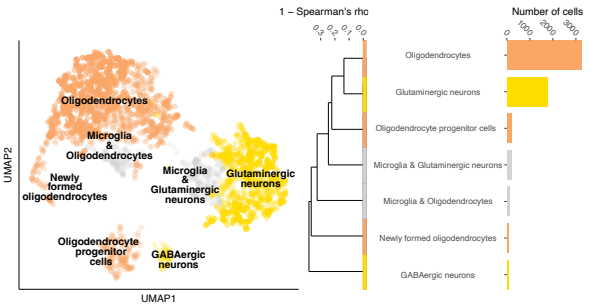

Occipital lobe_snRNA−seq

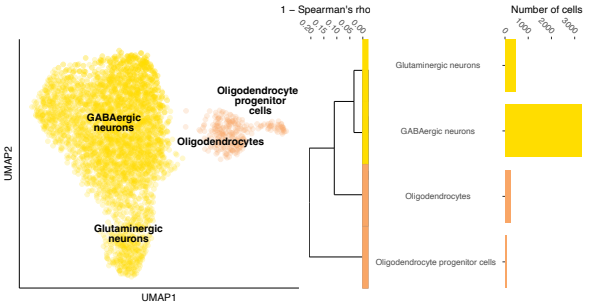

Parietal lobe_snRNA−seq

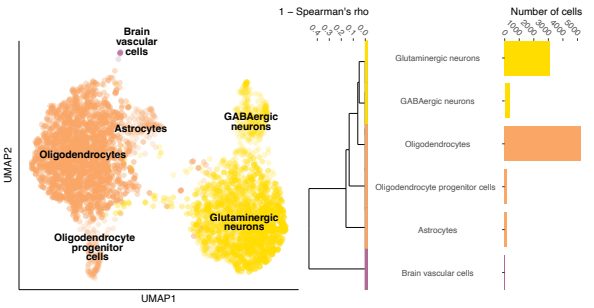

Temporal lobe_snRNA−seq

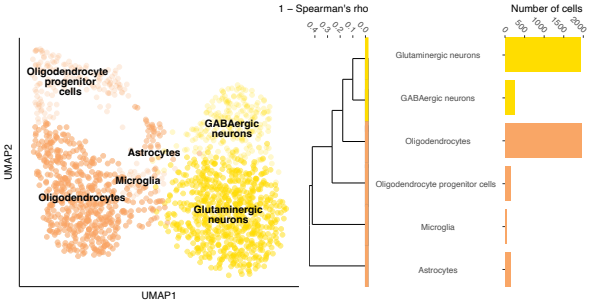

Cerebellum_snRNA−seq

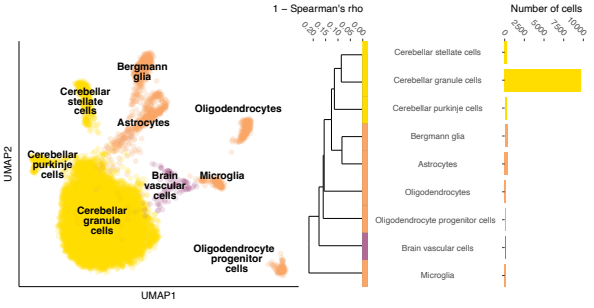

Hypothalamus_snRNA−seq

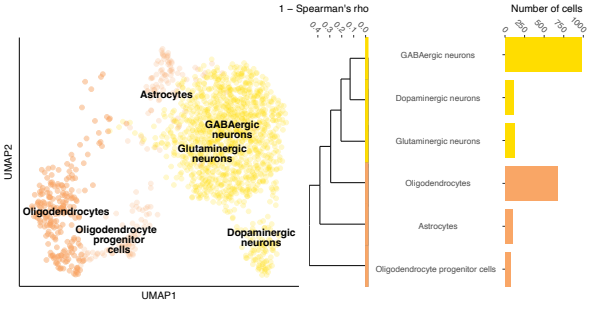

Subfornical organ_snRNA−seq

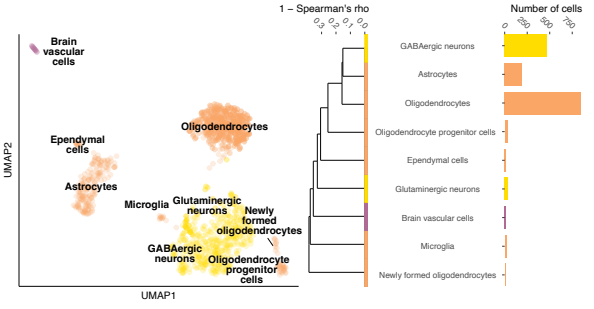

OVoLT_snRNA−seq

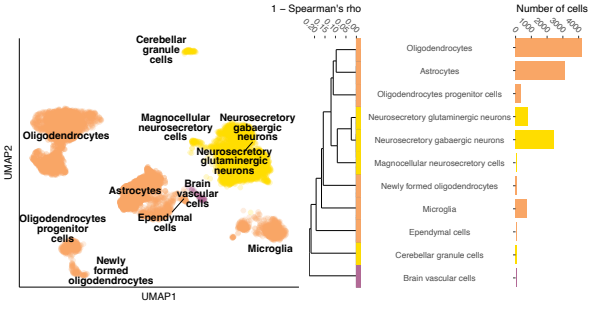

Area Postrema_snRNA−seq

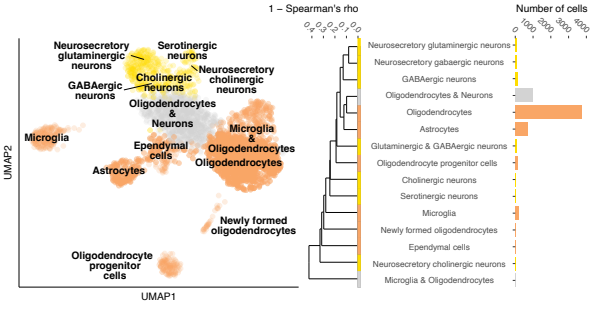

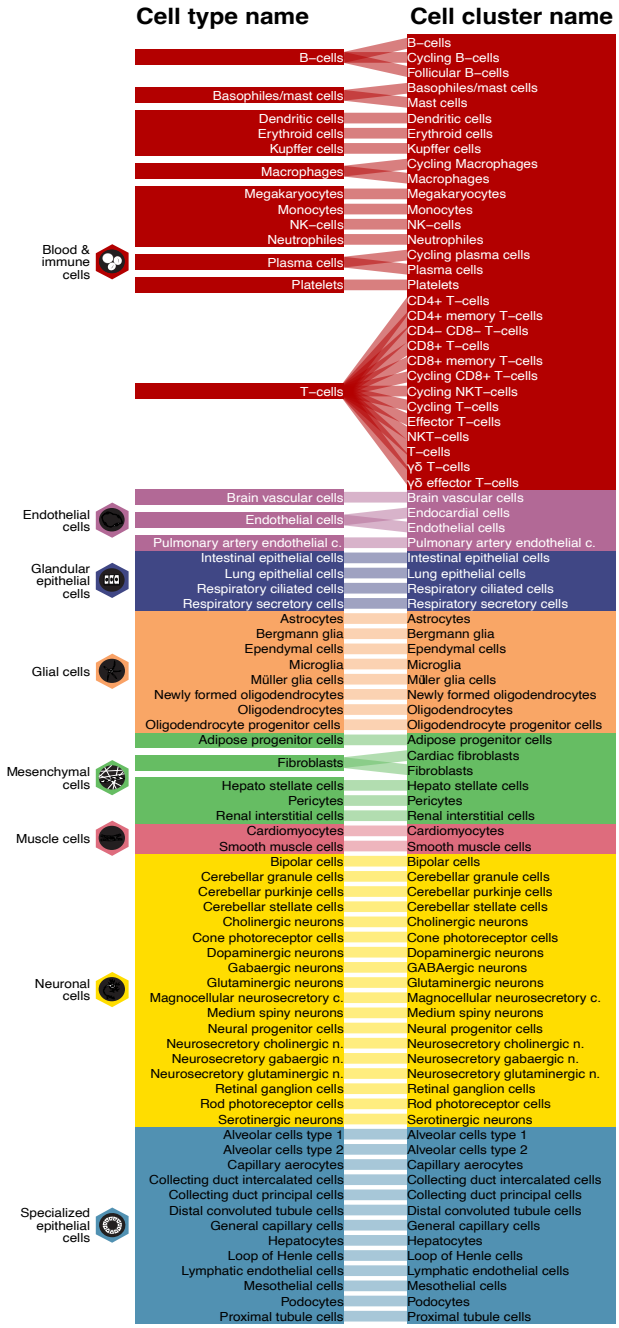

Figure S3. Renaming strategy for cell cluster names into cell type names.

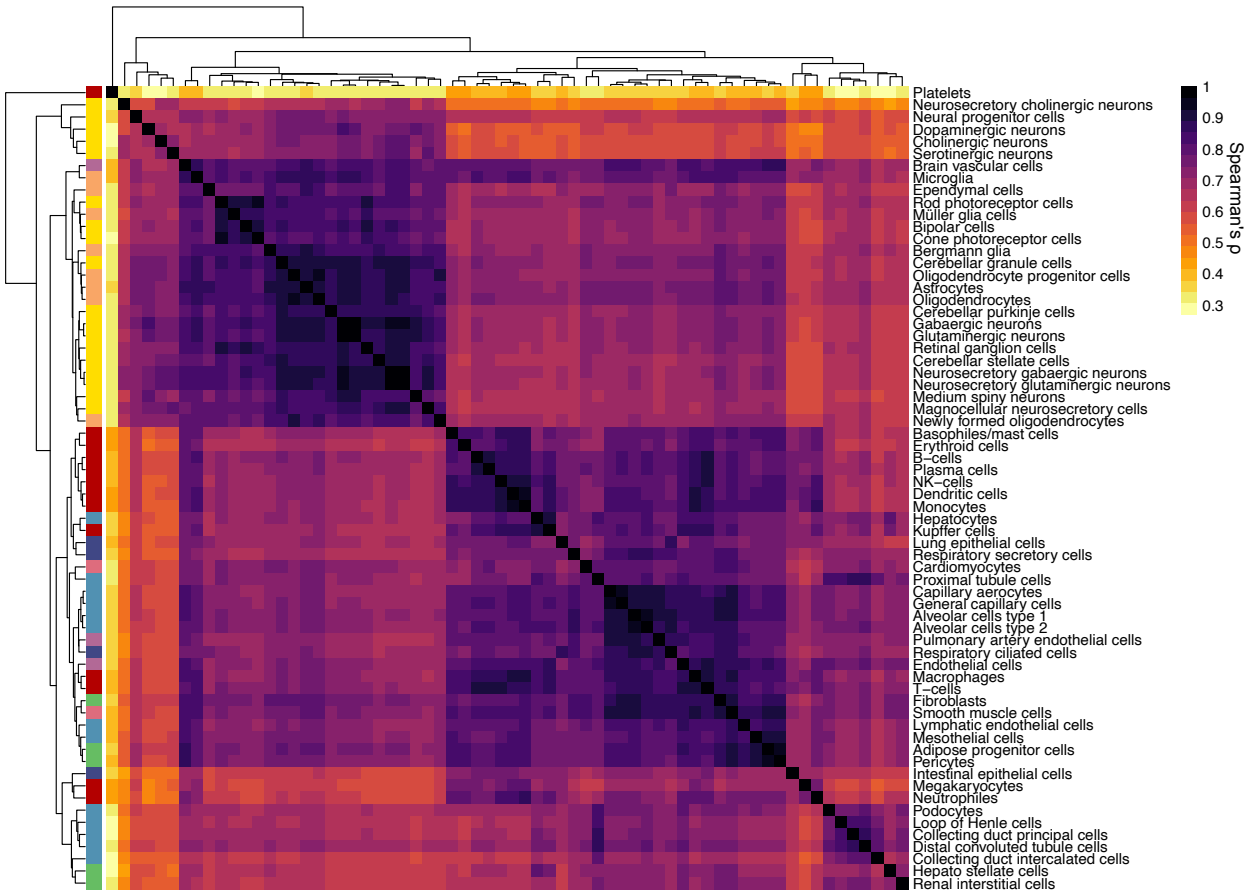

Figure S4. Clustered heatmap showing the pairwise spearman correlation between each cell type. Clustering calculated with complete linkage method.

Figure S5. Relative cell count identified for each cell type by tissue. A total of 66 cell types were identified across all 24 libraries or 20 tissues. Relative cell count was calculated as the quotient of the counts per cell type in a tissue and the total cell count of a tissue. For samples, which had both single cell and single nuclei libraries, the total cell count of a tissue was computed through first adding the total cell count in a sample together.

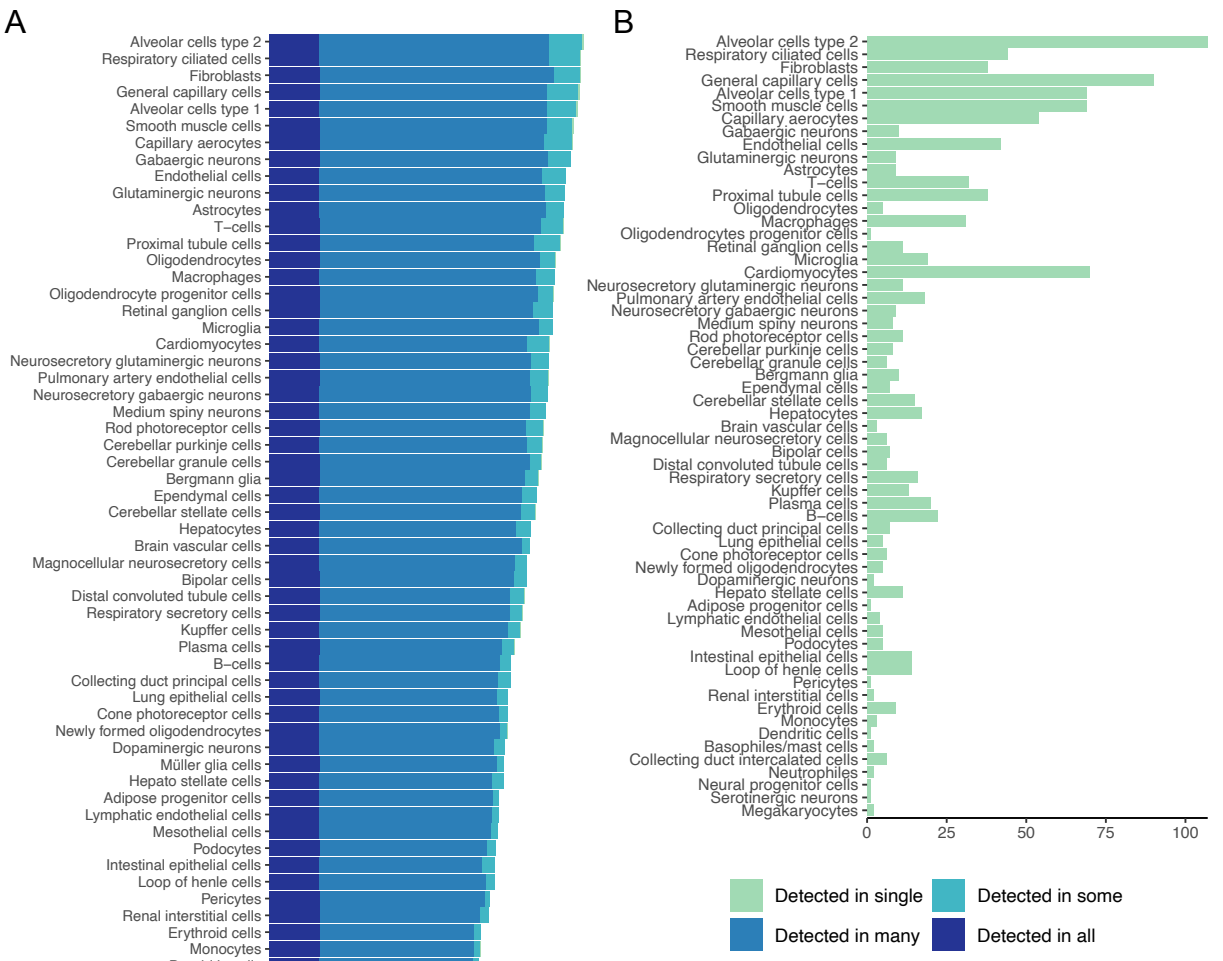

Figure S6. Gene distribution annotation annotation per cell type. A) For every cell type, the amount of genes annotated to each of the four distribution categories. B) Number of genes annotated as detected in single for for each cell type.

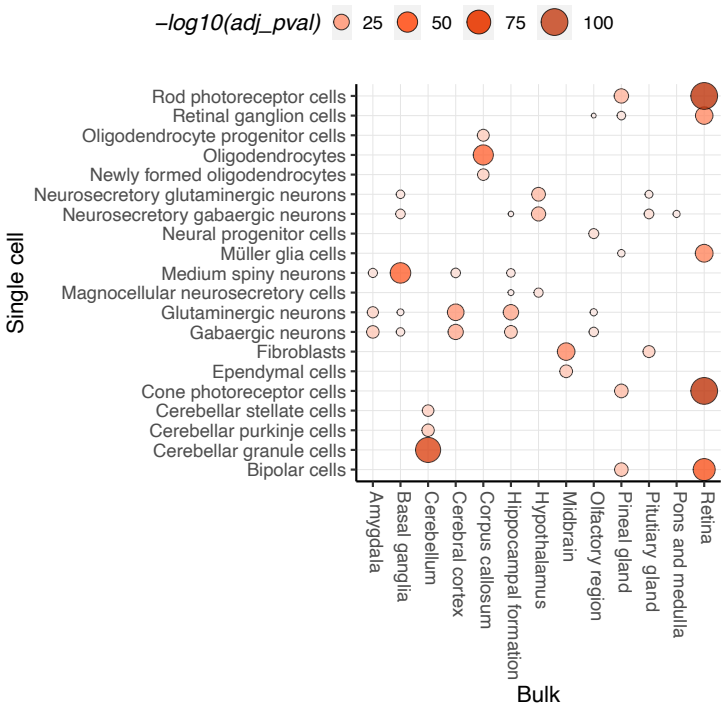

Figure S7. Hypergeometric test based on matching elevated genes between cell types detected in brain tissue and retina and bulk RNA tissue of regions located in the brain and the retina.

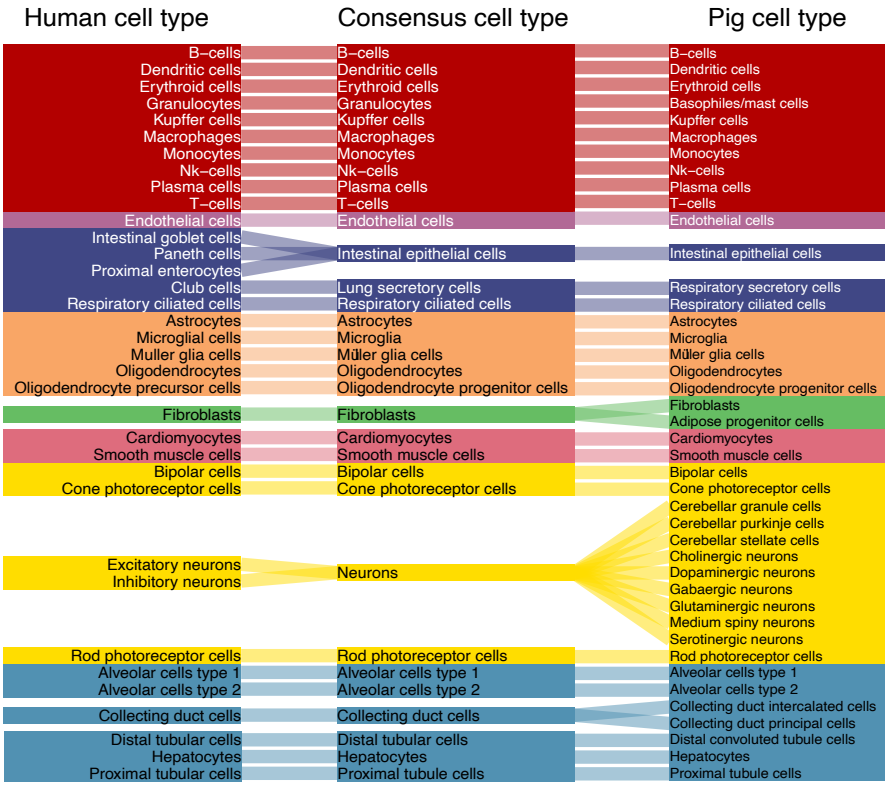

Figure S8. List of cell types pooled together in order to create a matching consensus cell type gene expression matrix used as a basis for the human to pig single cell type comparison. The consensus datasets were computed by taking the mean expression of every gene in a cell type assigned to matching consensus cell types. Only ortholog genes were included.